2D simulations of quasicrystals with patchy colloids

Master's Thesis in Physics

Presented by
Anja Gemeinhardt
October 5, 2018

Institute for Theoretical Physics 1
Friedrich-Alexander University Erlangen-Nürnberg

Supervisor: Prof. Dr. M. Schmiedeberg

Contents

1 Introduction

Recently, patchy particles attracted a lot of scientific interest. A patchy particle is a particle with varying interaction properties on its surface [16]. One example are atoms, e.g. carbon, which is known to form directional bonds thanks to its electronic orbitals [29]. Another example are so-called patchy colloids, e.g. Janus particles, proteins or macromolecules. In simulations patchy particles have been shown to self-assemble into various archimedean tilings [47] or dodecagonal quasicrystals [10, 35, 45]. In experiments a lot of progress has been made, regarding the synthesis of patchy colloids [4, 7, 49, 50]. For example the size and the position of patches on spherical particles can be influenced quite nicely. However, the large scale fabrication of patchy colloids remains challenging. Tian *et al*. managed a breakthrough in the production of ellipsoidal particles with controllable patches on large scales [43]. Possible areas of applications for colloidal structures in general lie in photonic crystals [22], targeted drug delivery [6, 21] or electronics [33, 34]. One possible future application may be the storage of information. Phillips *et al*. [33] examined colloidal clusters with Brownian dynamics simulations. They came to the conclusion, that clusters of N particles can store an amount of information going with $\mathcal{O}(N\ln N)$. Furthermore, those clusters are reconfigurable, such that information could be written, stored and erased. They confirmed their results in experiment for a cluster of $N = 4$ particles. Thus, if the self-assembly of colloids is understood and controllable, it might well be used in electronic devices in the future.

A class of structures that may be formed by patchy colloids are quasicrystals, i.e. structures that exhibit long-range positional and orientational order although they do not exhibit translational symmetry [40]. Quasicrystals possess additional degrees of freedom that lead to interesting material properties like plasticity as well as electronic and photonic properties [3, 9, 20, 23, 27, 46]. Aim of this thesis is to investigate a relatively simple model of patchy particles in simulations. We will explore how the width of the patches influences the structures that are formed by the particles. Hence, we find two metastable quasicrystalline phases. Furthermore, the growth of dodecagonal quasicrystals formed with patchy colloids will be compared to the growth of dodecagonal quasicrystals formed with isotropic particles. In both systems, we observe the growth of almost perfect quasicrystals. However, the patchy particles tend to form regions of phononic or phasonic displaced particles that are sometimes connected to dislocations.

2 Background

2.1 Quasicrystals

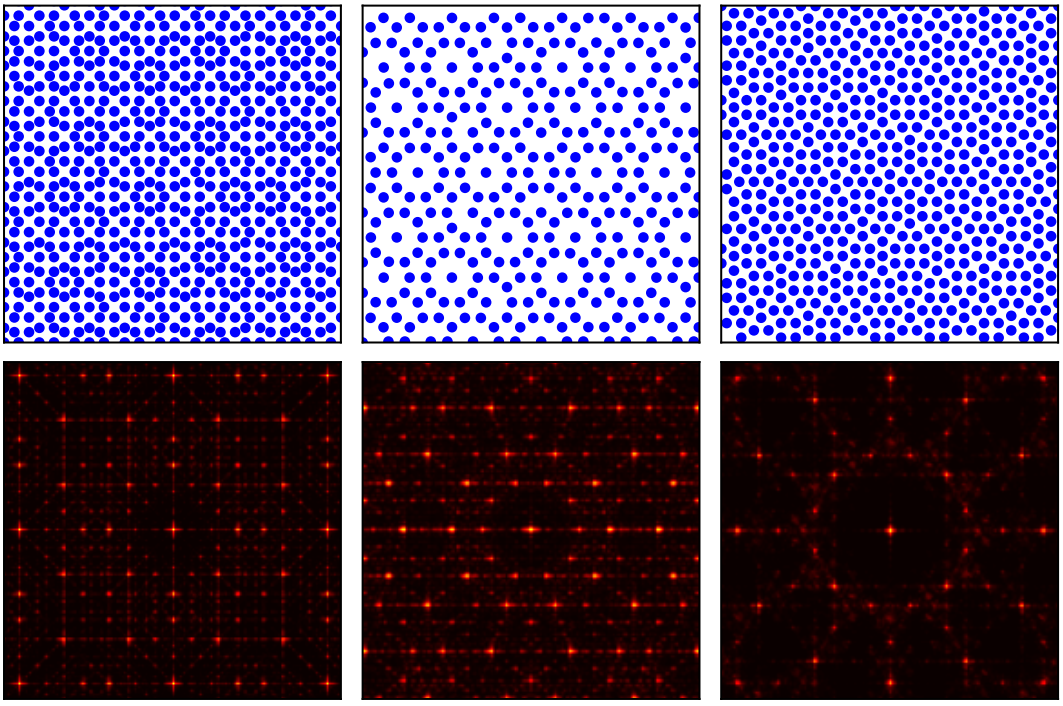

Figure 2.1: Examples of ideal quasicrystals with **a)** octagonal, **b)** decagonal and **c)** dodecagonal order. The upper row depicts the quasicrystal in real space, while the lower row depicts the according structure factor $S(q_x, q_y)$.

Periodic structures may only have 2-, 3-, 4- or 6-fold rotational symmetry [2]. Nevertheless, in 1984 Dan Shechtman discovered a structure with icosahedral symmetry, the first experimental observation of a quasicrystal [40]. In 2011 Shechtman's famous discovery was awarded a Nobel Prize in chemistry [1]. Since then many different quasicrystalline structures have been found, mostly in metallic alloys [42] or soft matter systems [11]. Quasicrystals do not exhibit translational symmetry, therefore they can not be described by any periodic

lattice. Examples of three important quasicrystalline tilings are illustrated in fig. 2.1, the octagonal Ammann-Beenker tiling, a decagonal tiling and the dodecagonal square-triangle tiling. Although none of these tilings can be described with a periodic lattice one can observe repeating arrangements of particles e.g. the Ammann-Beenker tiling (fig. 2.1**a)**) shows rings of eight particles around a central particle, similarly the decagonal tiling (fig. 2.1**b)**) shows rings of ten particles. The dodecagonal square-triangle tiling (see fig.2.1**c)**) lives up to its name as it solely consists of squares and triangles. However, symmetry and repeating particle arrangements are harder to observe in this dense tiling. Nonetheless, there are arrangements of one central particle surrounded by an inner ring consisting of six particles and an outer ring consisting of twelve particles.

Furthermore, as quasicrystals do not possess (periodic) translational symmetry, they need to have at least two incommensurate length scales. This can be seen exemplarily in fig. 2.1**b)**, the decagonal quasicrystal shows rings of ten particles whose distance to each other corresponds to the short length scale, while the distance to the central particle corresponds to the long length scale of the quasicrystal. In order to form the desired quasicrystal in simulations, one can choose a pair potential that supports the appropriate length scales [14, 15]. Alternatively, one can choose a pair potential with preferred bonding angles that only supports one of the length scales explicitly. Within this thesis we will examine the second approach.

2.1.1 Order parameters

Determining the orientational and positional order of any given structure is not an easy task. Therefore, we will discuss suitable order parameters in order to identify quasicrystals and their rotational symmetry. Firstly, we will introduce the radial pair correlation function $g(r)$, which measures variations of the particle density depending on a radius $r + dr$ around a reference particle. It is given by

$$g(\mathbf{r}) = \frac{V}{N}\langle\sum_{i\neq j}\delta(\mathbf{r} - (\mathbf{R_i} - \mathbf{R_j}))\rangle. \tag{2.1}$$

Thus, the radial pair correlation function $g(r)$ quantifies the positional order of a given structure, however, one can not determine orientational order using $g(r)$. Experimentally, the rotational symmetry of a solid can easily be seen in its diffraction pattern. The theoretical equivalent of a diffraction pattern is the so-called (static) structure factor $S(\mathbf{q})$. It can be calculated using a Fourier transformation of the pair correlation function $g(r)$ into momentum space

$$S(\mathbf{q}) = \frac{1}{N}\sum_{j,k=1}^{N}\exp(-i\mathbf{q}(\mathbf{r}_j - \mathbf{r}_k)). \tag{2.2}$$

Plotting the structure factor S in dependence of the wave vectors q_x and q_y corresponds to the diffraction pattern of a two-dimensional particle configuration. Peaks in the structure factor or accordingly in the diffraction pattern characterize positional order. The lower row of fig. 2.1 illustrates the diffraction patterns of the corresponding quasicrystals. Here, one can observe peaks which are arranged on rings around a central peak. The rotational symmetry can be determined by counting the peaks within one ring, e.g. the structure factor of the dodecagonal crystal clearly shows twelve peaks in each ring. However, one should be careful as, e.g. two triangular domains which are rotated about $\pi/6$ also show one central ring of twelve homogeneously distributed peaks although the structure does not show dodecagonal order. This phenomenon is called twinning.

Alternatively, one can determine a quantitative measure of a given rotational symmetry m by calculating the bond orientational order parameter

$$\psi_m(\mathbf{r}_j) = \frac{1}{N} \sum_{k \in NN} \exp(im\phi_{jk}) \tag{2.3}$$

where N denotes the number of nearest neighbours $NN = \{1, ..., N\}$ and ϕ_{jk} denotes the bond angle between particle j and particle k. If the bond angle fits to the rotational symmetry, i.e. $\phi_{jk} = l \cdot 2\pi/m$ where $l \in \mathbb{N}$ the exponential reads $\exp(im \cdot l \cdot 2\pi/m) = 1$. The average of the absolute values $|\psi_m|$ over a configuration is a quantitative measure of how good the particles are ordered according to m-fold rotational symmetry. Note, that this will also detect symmetries compatible to m-fold symmetry, i.e. 2m-fold, 3m-fold and so on.

Lastly, the angular distribution function $g_\phi(\phi)$ shows which bond angles are preferred between nearest neighbour particles. It reads

$$g_\phi(\phi) = \sum_{i=1}^{N} \sum_{\substack{k \in NN_i \\ l \in NN_{i,k}}} \delta(\phi - \phi_{kl}) \tag{2.4}$$

where NN_i denotes the nearest neighbours of particle i, $NN_{i,k} = NN_i \cap NN_k$ and ϕ_{kl} denotes the angle between the particles $\phi_{kl} = \angle lik$.

2.1.2 Dynamic properties

The dynamics of quasicrystals is determinated by two elementary excitations, phonons and phasons [41]. Phonon modes correspond to the oscillatory motion of particles around their equilibrium position, as in periodic crystals. More interesting are phason modes which arise due to additional degrees of freedom associated to new rotational symmetries possibly occuring due to the loss

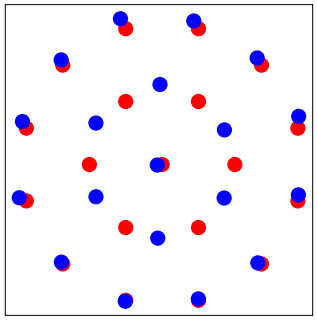

Figure 2.2: Sector of a particle configuration showing correlated phasonic flips in a local dodecagonal tiling. Particles coloured in red represent the original particle positions, blue the positions after a certain simulation time. Small fluctuations of the particle positions are due to thermal fluctuations.

of translational symmetry. Phasons describe correlated rearrangements of particles that do not cost free energy in the limit of long wavelengths [38]. The elementary process is a single phasonic flip where one particle moves to an energetically equivalent position corresponding to a short wavelength excitation [15,41]. Thus, phasonic flips rearrange one local configuration into a very similar configuration. An example of several correlated phasonic flips is depicted in fig. 2.2. Six correlated particles flip around a central particle, leaving the local configuration almost invariant. Furthermore, phasons are diffusive and, as a consequence, relax slowly. Phasons occur naturally during the growth process of quasicrystals and are believed to influence the healing of defects [28].

Topological defects occuring in crystals are so-called dislocations. In quasicrystals dislocations require a mixture of phononic and phasonic displacements and can be described as such [41]. They influence the mechanical properties of quasicrystals [12], e.g. the propagation of cracks in quasicrystals [9,27].

2.2 Patchy colloids

Colloids are particles whose size is roughly in the range of nanometres to micrometres. As the name patchy implies, patchy colloids possess varying interaction properties at their surface, e.g. differently charged regions. Promising applications of patchy colloids lie in photonic crystals or medicine [6,21,22]. A nice example, based on the self-assembly of patchy colloids, is the formation of a lens overcoming spherical aberration [5]. The underlying principle was discovered by examining squid eyes. Patchy proteins form gels of varying density such that a parabolic relationship between refractive index and lens

radius is achieved. Thus, the lens counters spherical aberration.

In order to use patchy colloids in applications it is important to understand and control their self-assembly. Therefore, we will shortly introduce studies examining the self-assembly from the experimental and respectively theoretical point of view.

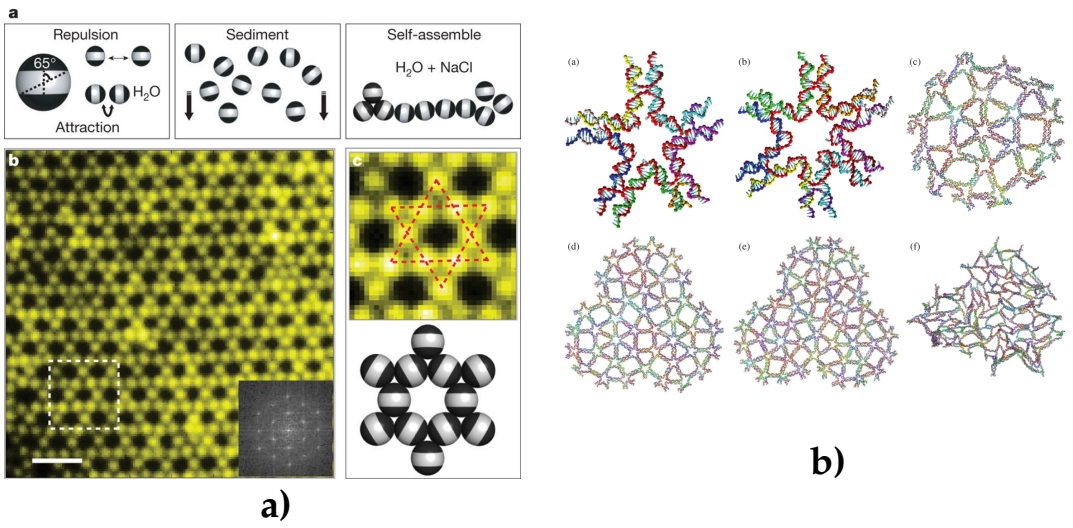

Figure 2.3: **a)** Self-assembly of patchy colloids in a Kagome lattice [8] **b)** Star-like DNA particles ((a) and (b)), that form motifs of a dodecagonal quasicrystal, when adsorbed onto a surface (c-e) and flexible motifs when free in solution (f) [36]

As an experimental example we will introduce a study by Chen *et al*. who conducted the self-assembly of tri-block Janus spheres, i.e. spherical particles with two opposing patches, into a Kagome lattice [8]. Fig. 2.3**a)** schematically depicts the experiment. The colloids were kept in deionized water in order to sediment. Then NaCl was added, which induces electrostatic repulsion and allows the patchy colloids to self-assemble. Thus, a Kagome lattice was formed (fig. 2.3**a)**).

On the theoretical side Reinhardt *et al*. simulated star like particles consisting of DNA strands (see fig. 2.3**b)**) [36]. When these particles are adsorbed onto a surface, they show motifs of a dodecagonal quasicrystal. However, due to the high flexibility of the DNA strands, they show fluxional motifs in a solution. All of their simulations were performed at 22°C. Thus, Reinhardt *et al*. have shown that it should be possible to form a soft DNA quasicrystal at room temperature by adsorbing artificially designed star like particles onto a surface.

3 Methods

3.1 Particle model

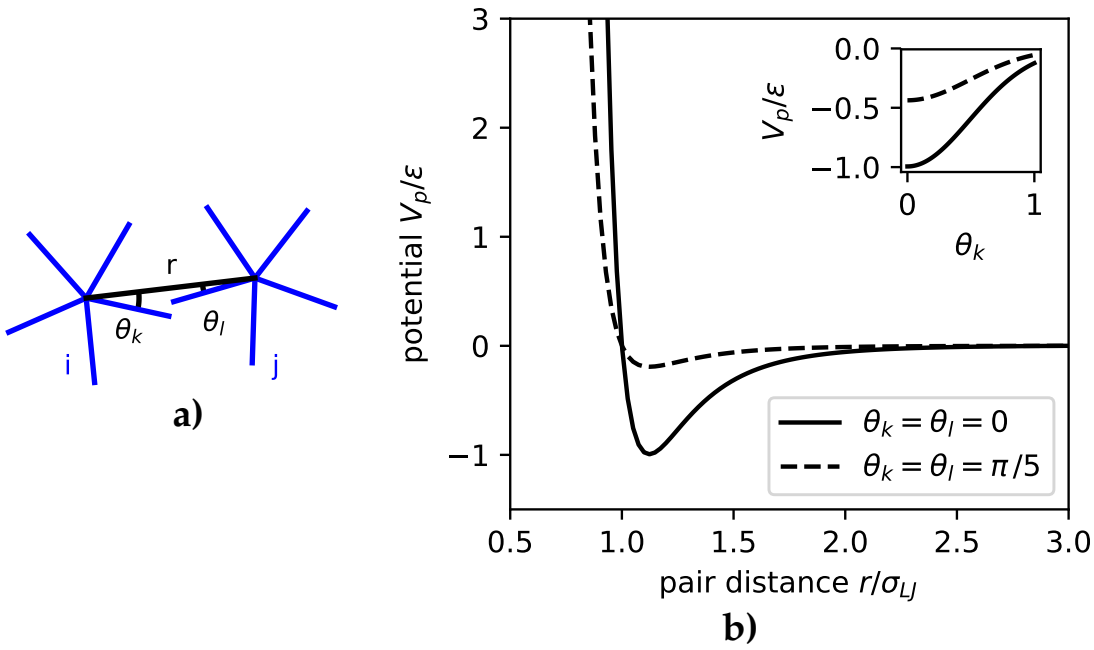

Figure 3.1: **a)** Representation of two particles i and j, with five regularly arranged patches. **b)** Pair potential V_p, the parameters read $\sigma_{LJ} = 1$, $n = 6$, $\sigma_{pw} = 0.49$. The continuous line shows the optimal case where the patches of two neighbouring particles face each other and the potential is minimal. The dashed line indicates the worst case where both patches have the maximal angle to the inter-particle vector, i.e. $\theta_k = \theta_l = \pi/5$ in the case of particles with five patches. The inset shows the dependence of the angle θ_k. Again, the continuous line indicates the optimal case where $\theta_l = 0$, while the dashed line indicates the worst case where $\theta_l = \pi/5$:

In order to simulate patchy colloids one can use a potential with one minimum, i.e. one length scale that achieves preferred bonding angles between the particles by using attractive patches. As far as we know the only quasicrystal found in literature by using this patchy potential exhibits twelve-fold

symmetry [10,35,45]. Aim of this thesis is to examine this approach of using patchy particles in order to form quasicrystalline structures. Note that this is particularly interesting due to the fact that within quasicrystals the particles have at least two incommensurate length scales. However, the patchy colloids as simulated in this thesis only support one length scale intrinsically. The other length scale has to be supported implicitly by the patches.

The patchy particles regarded within this thesis are two-dimensional disks with attractive patches. We will regard two different versions of the pair potential described below. Firstly, a potential that considers patches extending into the particle core V_p and secondly a potential that only models patches at the surface of the particle $V_{p,surf}$. Both potentials are modelled by using a simple modification of the Lennard-Jones pair potential. V_p is given by

$$V_p(r, \theta_k, \theta_l) = V_{LJ}(r) \cdot V^A \tag{3.1}$$

where V_{LJ} denotes the Lennard-Jones pair potential

$$V_{LJ}(r) = 4\epsilon \left[\left(\frac{\sigma_{LJ}}{r} \right)^{2n} - \left(\frac{\sigma_{LJ}}{r} \right)^{n} \right] = \epsilon \left[\left(\frac{r_0}{r} \right)^{2n} - 2 \left(\frac{r_0}{r} \right)^{n} \right]. \tag{3.2}$$

Here, r denotes the distance between the particles i and j. The equilibrium distance induced by this potential is given by $r_0 = \sqrt[n]{2}\sigma_{LJ}$. If not stated otherwise the exponent is chosen as $n = 6$. By modifying n one can modify the width of the minimum. The angular modification reads

$$V^A(\theta_k, \theta_l) = \exp(-\frac{\theta_k^2}{2\sigma_{pw}^2}) \exp(-\frac{\theta_l^2}{2\sigma_{pw}^2}) \tag{3.3}$$

where θ_k respectively θ_l denote the angles between the nearest patch of particle i respectively j to the inter-particle vector $\mathbf{r}_{ij}$, as illustrated in figure 3.1. The parameter σ_{pw} defines the width of the patches in radians. We will now introduce the maximum sensible patch width $\sigma_{pw,max}$, which is generally given by π divided by the number of patches, i.e. $\sigma_{pw,max} = \pi / N_{patches}$, where $N_{patches}$ denotes the number of patches. If σ_{pw} approaches $\sigma_{pw,max}$, the particle surface is completely covered by patches, i.e. the particles approach the form of isotropic particles. In the following, the distance r is given in units of r_0, temperature is given in ϵ / k_B and energy in ϵ.

The potential that only considers the patches at the surface $V_{p,surf}$ is given by

$$V_{p,surf}(r, \theta_k, \theta_l) = \begin{cases} V_{LJ}(r) & r \leq \sigma_{LJ} \\ V_{LJ}(r) \cdot V^A & r > \sigma_{LJ} \end{cases}. \tag{3.4}$$

Here the force, i.e. gradient of the pair potential is not continuous. Therefore, one cannot perform Brownian dynamics simulations using $V_{p,surf}$. However,

this potential has been examined in literature [10, 35, 45]. Thus, it is known, that particles with five (or seven) regularly arranged patches form dodecagonal quasicrystals at patch widths of about $\sigma_{pw} \approx 0.49 \approx 78\% \cdot \sigma_{pw,max}$.

3.2 Metropolis algorithm

The Metropolis algorithm is a type of Monte Carlo algorithm, that was introduced by Metropolis *et al*. in a paper from 1953 [25,26]. Aim of the algorithm is to sample energetically favourable configurations for a given system of particles within a given ensemble. In our simulations the systems are treated within the canonical (NVT) ensemble. The algorithm starts with a given, if not stated otherwise, random configuration of particles. It randomly selects a particle and tries a small displacement step. The size of this step is chosen randomly below a given maximum δr_{max}. As we are interested in patchy particles, a step can either be a displacement in $x-$ and $y-$direction or a rotation of the particle. Then, the algorithm compares the energies of the old and the new configuration. If $E_{new} \leq E_{old}$ the step is accepted, otherwise the step is accepted with a probability of

$$p = e^{-\beta(E_{new}-E_{old})} \quad \text{with} \quad \beta = \frac{1}{k_B T} \tag{3.5}$$

where E denotes the inner ennergy of a given configuration. This procedure is repeated until the simulation reaches thermal equilibrium. Note that the choice of the acceptance probability eq. (3.5) satisfies the detailed balance condition, i.e.

$$\frac{p_{i\to j}}{p_{j\to i}} = \frac{p_j}{p_i} \tag{3.6}$$

where p_i is the probability to be in configuration i [17]. Thus the algorithm minimizes the energy of the system. By allowing steps that result in slightly higher energies it is possible to get from one local minimum of the energy landscape to another. In the case of an ergodic system where all possible configurations are explored the probability to get configuration i from the algorithm is proportional to $\exp(-\beta E_i)$ [37]. However it is not possible to say whether a configuration found with this method belongs to a global minimum of the energy landscape or not, i.e. we can not be sure whether the resulting configuration is a stable or a metastable phase.

In our simulations the ratio of displacements to rotations is 1:1. The acceptance rates of displacements and rotations are adjusted separately, such that they are about 50%. This is realised by increasing the maximum value δr_{max} of trial steps, if the acceptance rate is larger than 50%. Otherwise, if the acceptance rate drops below 50% the maximum size of the steps is decreased. Acceptance rates of about 50% are presumably a good choice [17,37,39]. On one hand, an

acceptance rate of 50% guarantees that a large number of configurations around a (local) minimum of the energy landscape are explored. On the other hand it is still possible to escape one (local) minimum and reach another by increasing the step size. It should be noted that in case of the rotations the acceptance rates sometimes are quite high. This is due to the fact that rotations result in comparably small energy differences.

3.3 Brownian dynamics

Brownian dynamics is a useful method to describe the motion of particles in simulations. The underlying equation is also known as overdamped Langevin equation due to the neglect of inertia. Therefore, it is only applicable for systems with small mass or large viscosity.

$$\gamma \dot{\mathbf{x}} = \mathbf{F}_{int} + \mathbf{F}_T \tag{3.7}$$

γ denotes the friction coefficient, given by $\gamma = 6\pi\eta r_0$ where η denotes the dynamic viscosity. Thus, the first term of eq. 3.7, $\gamma\dot{\mathbf{x}}$, represents a frictional force between a particle and the solvent. The internal force $\mathbf{F}_{int}$ in eq. 3.7 is given by the gradient of the applied pair potential

$$\mathbf{F}_{int,i} = \sum_{j \neq i} -\nabla V_{ij}(\mathbf{x}). \tag{3.8}$$

The third term of eq. 3.7, $\mathbf{F}_T$, considers thermal motion of the particle. It has to comply with

$$\langle \mathbf{F}_T \rangle = 0 \tag{3.9}$$

$$\text{and } \langle \mathbf{F}_{T,i}(t)\mathbf{F}_{T,j}(t') \rangle = 2\gamma k_B T \delta_{ij}\delta(t-t'). \tag{3.10}$$

This is achieved by using Gaussian distributed random numbers with the requested properties. The algorithm integrates over equation 3.7 numerically i.e. $\Delta\mathbf{x} = \frac{\Delta t}{\gamma} \cdot \mathbf{F}$. Δt is chosen as $10^{-4}\tau_B$ where $\tau_B = \frac{\sigma_{LJ}\gamma}{\epsilon}$ denotes the Brownian time. Additionally, patchy particles experience a torque depending on their orientation θ. We calculate the torque on the particles analogous to eq. 3.7

$$\gamma_\theta \dot{\boldsymbol{\theta}} = \mathbf{M}_{int} + \mathbf{M}_T. \tag{3.11}$$

Note that the friction coefficient γ is replaced by the rotational friction coefficient γ_θ

$$\gamma_\theta = 8\pi\eta r_0^3 = \frac{4}{3} r_0^2 \gamma. \tag{3.12}$$

The internal torque is given analogous to the internal force and reads

$$\mathbf{M}_{int,i} = \sum_{j \neq i} -\frac{\partial}{\partial \theta} V_{ij}(r, \theta, \theta_l). \tag{3.13}$$

The thermal torque $\mathbf{M}_T$ has to fulfil the same conditions as the thermal force, see eq. 3.9 and eq. 3.10, with γ replaced by γ_θ. Lastly, the friction coefficients γ and γ_θ have to be determined such that the particles show the correct translational and rotational diffusion behaviour [18,31,32]

$$\langle r^2 \rangle = 4\frac{k_B T}{\gamma} \cdot t \quad \text{and} \quad \langle \theta^2 \rangle = 2\frac{k_B T}{\gamma_\theta} \cdot t. \tag{3.14}$$

Unfortunately, one has to consider the dependencies between x, y, and θ in order to determine the gradient analytically. Therefore, we calculate the displacements of the particles numerically by using the difference quotient, i.e. $F_{int,n} = \frac{V(n+dn)-V(n)}{dn}$ where $n \in \{x, y\}$.

3.4 Simulation box

Periodic boundary conditions are applied to all simulation boxes. As quasicrystals are aperiodic, one has to be careful to choose the size of the box such that a good approximation of the quasicrystalline pattern can form within the periodic boundaries. This can be achieved if multiples of all supported length scales fit in the box size. One approach to obtain appropriate box sizes is to minimize the discontinuity a particle within a quasicrystalline pattern experiences if it crosses the boundary [37,39].

In case of a dodecagonal structure one needs twelve reciprocal lattice vectors $\mathbf{G}_j = G \cdot (cos(2\pi j/12), sin(2\pi j/12))$ with length $G = 2\pi/r_0$ in order to construct a continuous quasicrystal. As twelve-fold symmetry is invariant under rotations of $\pi/2$ we can use a square box and it is sufficient to consider, e.g. the x-direction in order to choose its length in a suitable way, as described in the following. The length scales are given by the reciprocal lattice vectors $2\pi/G_{x,0} = r_0$, $2\pi/G_{x,1} = 2r_0/\sqrt{3}$, and $2\pi/G_{x,2} = 2r_0$. Therefore, multiples of $2r_0/\sqrt{3}$ should fit into the simulation box, i.e. we can use boxes with edge length $L = 2mr_0$ where approximately $m \cdot \sqrt{3} \in \mathbb{N}$. Hence, suitable values for m are $\{4, 11, 15, 19, 26, ...\}$.

Similarly, in case of an octagonal structure one can also use a square box. Again, it is sufficient to look at the x-direction of the reciprocal lattice vectors $2\pi/G_{0,x} = r_0$, $2\pi/G_{1,x} = \sqrt{2}r_0$. We can use a continuous fraction approximation

$$\sqrt{2} = \lim_{n \to \infty} \frac{P_{n+1} + P_n}{P_n} \tag{3.15}$$

where P_n are elements of the Pell sequence which is constructed by $P_0 = 0$, $P_1 = 1$ and $P_n = 2P_{n-1} + P_{n-2}$. Therefore, suitable box sizes are given by $L = mr_0$ where $m = P_{n+1} + P_n \in \{1, 3, 7, 17, 41, ...\}$.

Lastly, in case of a decagonal structure we can not use a square box. Therefore, we have to consider x- and y-direction $2\pi/G_{x,0} = r_0$, $2\pi/G_{x,1} = 2\tau r_0$ and $2\pi/G_{y,0} = r_0/\tau/\sin(\pi/5)$, $2\pi/G_{y,1} = r_0/\sin(\pi/5)$. Where τ is the golden mean which can be approximated by successive elements of the Fibonacci sequence

$$f_n = \begin{cases} f_{n-1} + f_{n-2} & \text{if } n > 2 \\ 1 & \text{otherwise} \end{cases} \tag{3.16}$$

Consequently, suitable edge lengths are $L_x = 2f_n r_0$ and $L_y = 2f_m r_0/\sin\left(\frac{\pi}{5}\right)$.

4 Complex structures

In this chapter we will reproduce the dodecagonal quasicrystal studied by Reinhardt *et al*., Doppelbauer *et al*. and van der Linden *et al*. [10,35,45]. Then, we will form a honeycomb lattice with patchy particles. In order to do this, we need to extend the pair potential such that the angular modification has two patch widths. Next, we use our knowledge of the pair potential and manage to examine a metastable decagonal and s metastable octagonal quasicrystal.

4.1 Dodecagonal quasicrystal

First, we test our algorithms, namely the Metropolis Monte Carlo and the Brownian dynamics algorithm, by reproducing the dodecagonal quasicrystal. We start testing the Metropolis algorithm by applying the pair potential with patches at the surface as given by eq. 3.4 and the pair potential with patches, that extend into the particle as given by eq. 3.1. In both cases we find the dodecagonal quasicrystal using particles exhibiting five regularly arranged patches with a width of $\sigma_{pw} = 0.49$. The melting point of both systems is approximately at $T_{melt} \approx 0.19$ which is in agreement with literature. Thus we ensure, that both potentials lead to similar results in the temperature regime of interest, i.e. $T \in [0.12; 0.22]$.

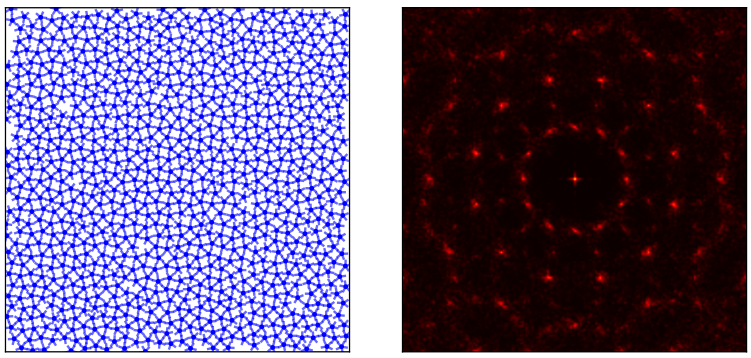

a) **b)**

Figure 4.1: **a)** Imperfect dodecagonal quasicrystal, obtained via Brownian Dynamics simulation at $T = 0.12$, $\sigma_{pw} = 0.49$, $N = 924$. **b)** Structure factor of **a)**

Furthermore, we test the Brownian Dynamics simulation using the same system parameters. As the force needs to be continuous, we could only apply the potential with patches extending into the particle (see eq. 3.1). Again, the dodecagonal quasicrystal forms for temperatures $T \leq 0.18$, a typical result is depicted in fig. 4.1. The melting point is the same as the one obtained using the Metropolis algorithm $T_{melt} \approx 0.19$.

4.2 Honeycomb lattice

One of the questions addressed in this thesis is, if one can find other quasicrystals using patchy particles. In order to do so we first want to obtain a better understanding of our potential. Therefore, we try to form the honeycomb lattice using particles exhibiting three patches. This lattice has already been found by Doppelbauer *et al*. [10], using the potential described in eq. 3.1. However, their simulations were based on a genetic algorithm. Using our Monte Carlo simulation we do not find the honeycomb lattice. Therefore, we extend the angular modification factor to

$$V_{ext}^{A} = \exp(-\frac{\theta_k^2}{2\sigma_{pw\,1}^2}) \exp(-\frac{\theta_l^2}{2\sigma_{pw\,1}^2}) + \exp(-\frac{\theta_k^2}{2\sigma_{pw\,2}^2}) \exp(-\frac{\theta_l^2}{2\sigma_{pw\,2}^2}) - \zeta. \quad (4.1)$$

The pair potential reads

$$V_{p,surf}(r, \theta_k, \theta_l) = \begin{cases} V_{LJ}(r) & r \leq \sigma_{LJ} \\ V_{LJ}(r) \cdot V_{ext}^{A} & r > \sigma_{LJ} \end{cases} . \quad (4.2)$$

The potential now uses two patch widths $\sigma_{pw\,1}$ and $\sigma_{pw\,2}$. Thus, the energy gain of two patches facing each other is larger. Within the simulation the two patches can be used in order to try a fairly narrow patch width $\sigma_{pw\,1}$, while ensuring that the patches still find each other by using a rather wide patch width $\sigma_{pw\,2}$. The inset of fig. 4.2 depicts the dependence of $V_{p,surf}$ on the particle orientation θ_k where the patch widths were chosen as $\sigma_{pw\,1} = 0.15$ and $\sigma_{pw\,2} = 0.7$. The offset $\zeta = 0.2$ causes a repulsive potential if both of the patch angles θ_k, θ_l are sufficiently large. Fig. 4.2 depicts such a case. At large patch angles $\theta_k = \theta_l = \pi/3$ the potential $V_{p,surf}$ shows a maximum, instead of a minimum, at $r = r_0$. Thus, large patch angles are actively suppressed by the pair potential. One should note that the offset ζ can cause V_{ext}^{A} to be negative. Therefore, it should only be applied to systems that use patches exclusively at the surface of the particles (see eq. 3.4). Otherwise, when applying the pair potential V_p (eq. 3.1) with patches extending into the particle core, particle distances smaller than the particle diameter might be preferable for sufficiently large patch angles.

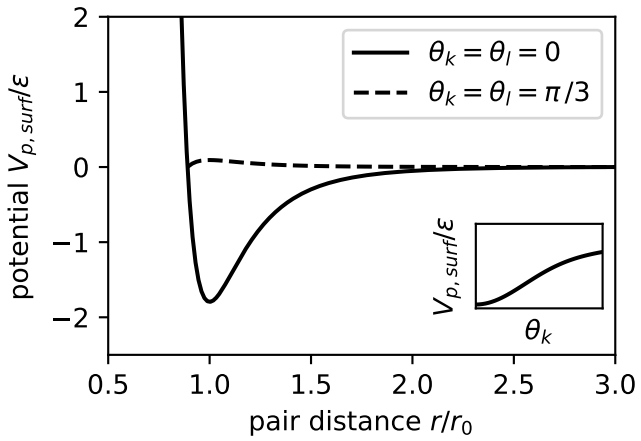

Figure 4.2: We depict the pair potential $V_{p,surf}$ with an extended angular modification factor. The potential parameters read $r_0 = 1$, $n = 6$, $\sigma_{pw1} = 0.15$, $\sigma_{pw2} = 0.7$ and $\zeta = 0.2$.

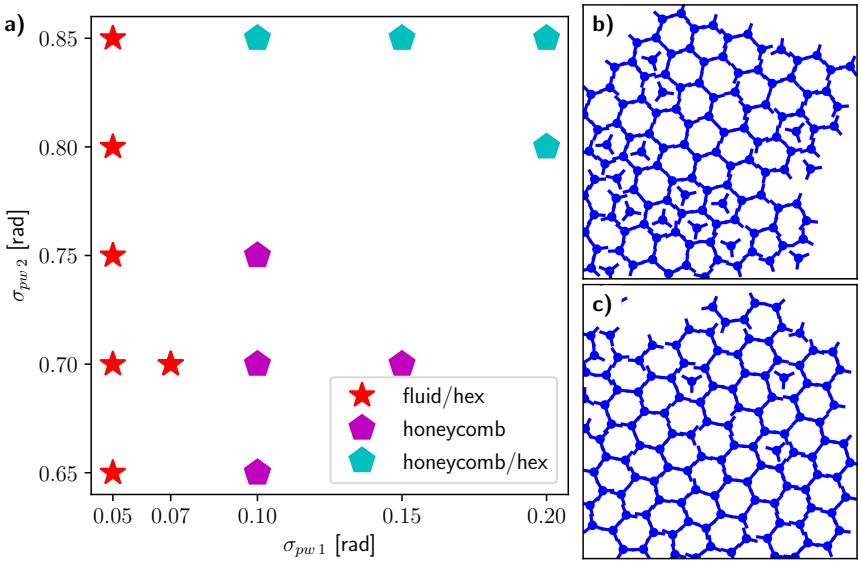

Figure 4.3: **a)** Phase diagram depending on the width of the patches obtained at $T = 0.23$, $\zeta = 0.2$, $N = 130$. **b)** Typical configuration depicting a mixture of hexagonal and honeycomb phase. We obtained this structure at $\sigma_{pw1} = 0.85$ and $\sigma_{pw2} = 0.2$. **c)** Typical configuration depicting a honeycomb lattice, obtained at $\sigma_{pw1} = 0.7$, $\sigma_{pw2} = 0.15$. Particles are depicted with patches.

By using this extended angular modulation, we are able to find the honeycomb phase (see fig. 4.3**c)**) with random initial configurations. Fig. 4.3**a)** shows the phase diagram at $T = 0.23$ and $\zeta = 0.2$ in dependence of both patch widths $\sigma_{pw\,1}$ and $\sigma_{pw\,2}$. In case of large patch widths $\sigma_{pw\,2} \gtrsim 0.8 \approx 76\% \cdot \sigma_{pw,max}$ high patch angles are obviously more likely. In this case the maximum sensible patch width, i.e. the width where particles approach isotropic form, is given by $\sigma_{pw,max} = \frac{\pi}{3}$. Additionally, the (repulsive) influence of the offset ζ is reduced, i.e. the energy penalty for forming high patch angles is low. Thus, the favourable phase in this regime seems to be a mixture of honeycomb and hexagonal lattice (fig. 4.3**b)**). Apparently the honeycomb lattice is also not favoured if the narrow patch width $\sigma_{pw\,1}$ is chosen too small. Finally, in an intermediate regime, where $\sigma_{pw\,1} \in [0.1; 0.15]$ and $\sigma_{pw\,2} \in [0.65; 0.75]$, the honeycomb lattice is preferred. Now, we can do a simple estimate

$$\begin{aligned} \sigma_{pw\,1} &= 0.10 \mathrel{\widehat{=}} 9.5\%\ \sigma_{pw,\,max} \\ \sigma_{pw\,2} &= 0.75 \mathrel{\widehat{=}} 71.6\%\ \sigma_{pw,\,max} \end{aligned} . \tag{4.3}$$

Thus, we can guess suitable values for $\sigma_{pw\,1}$ and $\sigma_{pw\,2}$ in order to find more interesting phases, e.g. decagonal or octagonal quasicrystals.

4.3 Decagonal quasicrystal

In the following section, we try to stabilize a decagonal quasicrystal as illustrated in fig. 2.1 and explore the dependence of the structure on the patch width. Thus, we use particles exhibiting ten regularly arranged patches. The decagonal quasicrystal supports two characteristic length scales $l_0 = 1$ and $l_1 = \frac{1+\sqrt{5}}{2} \approx 1.62$. However, we want to stabilize it using a pair potential that only has one minimum. It is known that the dodecagonal quasicrystal is stabilized by using a pair potential that supports the short length scale of the dodecagonal quasicrystal $r_0 = l_0$. Therefore, we also start by supporting the short length scale of the decagonal quasicrystal. Note that in case of the dodecagonal square-triangle tiling the formation of the long length scale occurs between second neighbours such that first neighbours can exclusively form distances of the short length scale. However, this is not possible for the decagonal quasicrystal that we aim to stabilize. Therefore, we lower the energy cost for supporting the other length scale by lowering the gradient of the pair potential, i.e. we choose a Lennard-Jones exponent of $n = 2$ (see eq. 3.2). In the following sections 4.3 and 4.4 we always use the extended angular modulation factor V_{ext}^{A} as given in eq. 4.1 without an offset, i.e. with $\zeta = 0$.

4.3.1 Supporting the short length scale

Here we use a potential with patches only at the surface $V_{p,surf}$ as given in eq. 4.2. We choose the parameters of $V_{p,surf}$ as $r_0 = 1$, $n = 2$, $\sigma_{pw\,2} = 0.23$, i.e. we support the short length scale of the tiling while applying a rather flat potential minimum and a wide patch width $\sigma_{pw\,2}$.

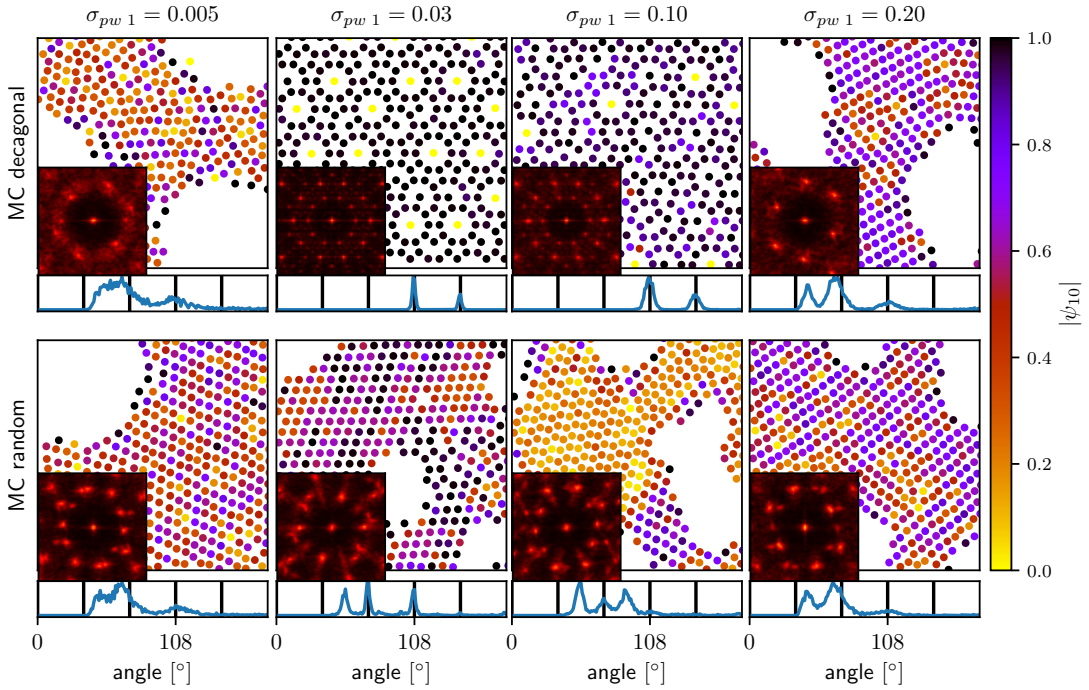

Figure 4.4: Configurations obtained after $2E8$ MC steps with an initial decagonal quasicrystal (upper row) and an initial random configuration (lower row) for different patch widths $\sigma_{pw\,1}$ (columns). The color code illustrates the bond orientational order parameter $|\psi_{10}|$. The insets depict the according structure factor. The graphs below the structures show the according angular distribution functions. The black lines serve as guide to the eye to indicate ideal decagonal angles, i.e. angles of $\{i \cdot 2\pi/10,\ i \in \mathbb{N}\} = \{36°, 72°, 108°, 144°, ...\}$. All simulations were done at $T = 0.2$, $N = 644$.

We run our MC simulation with different input structures, namely decagonal, square, triangle and a random structure, and analyse the resulting structures in dependence of the patch width. As we aim to form the decagonal tiling, all of the initial configurations were chosen at approximately the same density as the ideal decagonal tiling, i.e. $\rho \approx \rho_{10} \approx 0.63$. Typical structures and their angular distributions are shown in fig. 4.4. The decagonal tiling remains stable at narrow patch widths $0.005 < \sigma_{pw\,1} \approx 0.1$. At $\sigma_{pw\,1} = 0.1$ the particles start to rearrange and the peaks of the angular distribution function are broadened.

Random, square and hexagonal initial configurations result in the same final structures. Therefore, we show typical results obtained with a random initial configuration. As the density of the quasicrystal is rather low, the resulting structures exhibit large gaps, i.e. they coincide with a gas-like phase. At very low patch widths $\sigma_{pw\,1} = 0.03$ the angular distribution shows two peaks supporting decagonal symmetry at 72° and 108° and one peak at 54°. Most of the particles are ordered in a dense periodic structure. Furthermore, one can observe the rare formation of pentagons. At intermediate patch widths $\sigma_{pw\,1} = 0.1$ this dense structure competes with an Archimedean $(3^3 4^2)$ tiling. In the angular distribution the peak at 108° vanishes and a new peak emerges at approximately 90°. At high patch widths, e.g. $\sigma_{pw\,1} = 0.2$, the resulting structure does no longer depend on the initial structure. Both decagonal and random initial structures result in a dense phase, that supports angles of approximately 45° and 66°.

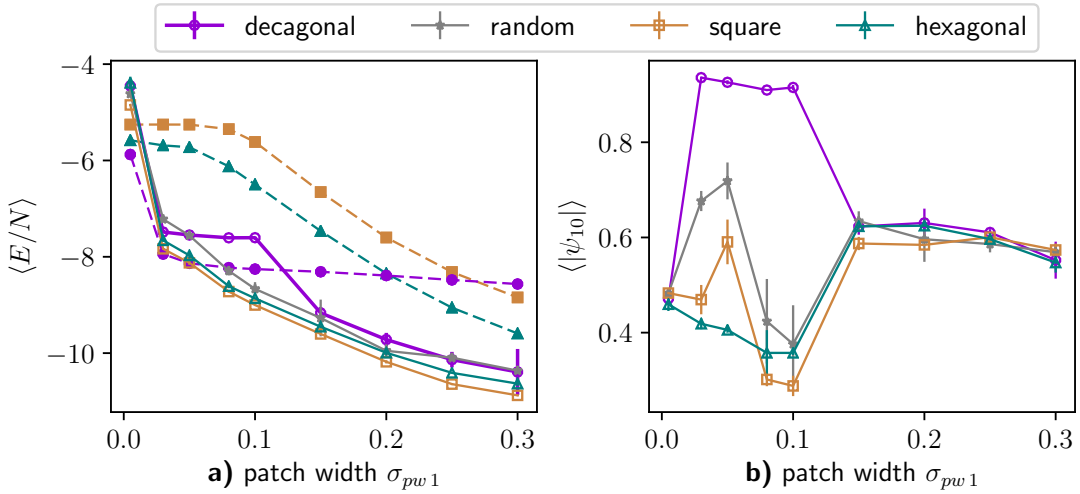

Figure 4.5: **a)** Energy per particle of the ideal structures (filled markers) and accordingly the structures formed after $2E8$ MC steps (hollow markers). **b)** Average of the bond orientational order parameter $\langle |\psi_{10}| \rangle$.

In fig. 4.5 we depict the average mean energy per particle $\langle E/N \rangle$ and the bond orientational parameter $\langle |\psi_{10}| \rangle$ in dependence of the patch width $\sigma_{pw\,1}$. At very narrow patch widths $\sigma_{pw\,1} = 0.005$, the potential minimum is very thin and therefore the curvature is large. The probability of particles escaping that minimum increases with increasing curvature and temperature. Consequently we observe structures of high energy and low ten-fold orientational order at $\sigma_{pw\,1} = 0.005$. In the regime of narrow patch widths $0.005 < \sigma_{pw\,1} \lesssim 0.1$ the structures with an initial decagonal tiling show high decagonal order. However, the energy per particle is higher than the energy per particle of the denser structure that forms when using other initial structures. Thus we conclude that

the decagonal phase is metastable at narrow patch widths. At higher patch widths the stable structure is a dense phase which predominantly forms angles of 45° and 66°.

4.3.2 Supporting the long length scale

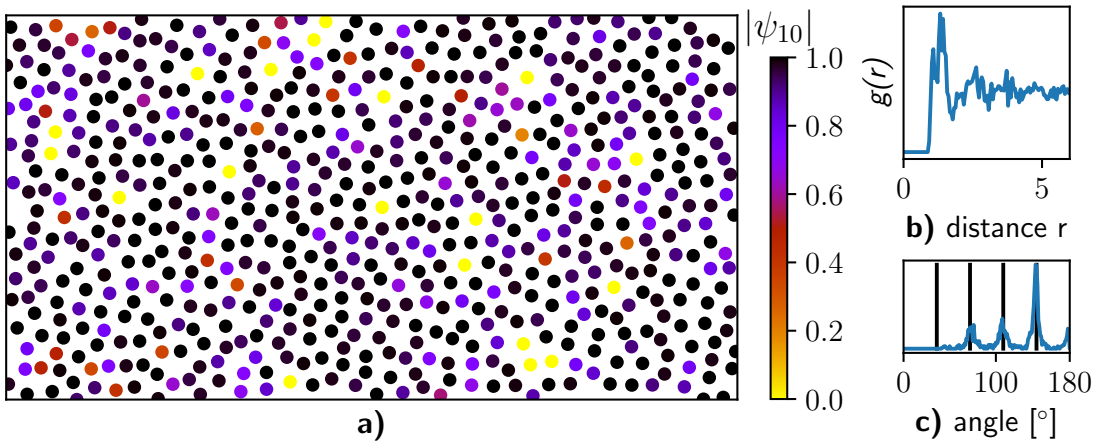

Figure 4.6: **a)** Structure obtained at $T = 0.2$, $N = 644$. The color code illustrates the bond orientational order parameter $|\psi_{10}|$ of the particles. **b)** depicts the according pair correlation function $g(r)$. Furthermore, we depict the according angle distribution in **c)**. Again, the black lines indicate angles suitable to decagonal symmetry.

Here we examine the behaviour of the system with the potential minimum applied at the long length scale of the decagonal quasicrystal. Thus, we choose the equilibrium distance as $r_0 = l_1 \approx 1.62$. We apply the potential V_p with patches extending into the particle such that the potential still induces preferred bond angles at $r = l_0$. Fig. 4.6 shows a typical structure obtained with an initial random configuration of the same density as the decagonal tiling $\rho = \rho_{10} \approx 0.63$. We choose the same potential parameters as in the previous section, i.e. $n = 2$, $\sigma_{pw\,1} = 0.03$, $\sigma_{pw\,2} = 0.23$. The resulting structure, as illustrated in fig. 4.6**a)**, shows a high ten-fold orientational order, measured by $\langle|\psi_{10}|\rangle \approx 0.90$. Furthermore, the angular distribution (fig. 4.6**c)**) shows peaks exclusively at angles suiting to decagonal symmetry. However, regarding the particle positions one can not detect a clear structure. In fig. 4.6**b)** we depict the pair correlation $g(r)$ which shows that the structure does not exhibit long-range positional order. We conclude that the patchy particles form a fluid or an amorphous solid.

4.4 Octagonal quasicrystal

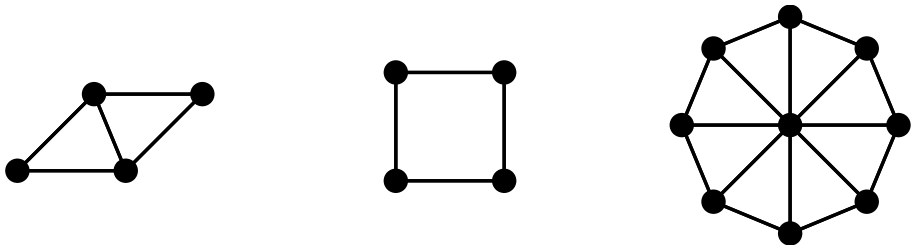

a) rhomb **b)** square **c)** ring

Figure 4.7: Basic tiles of the Ammann-Beenker tiling **a)** a rhomb and **b)** a square. A typical local octagonal arrangement is the ring depicted in **c)**, it consists of eight (half) rhombs.

The basic tiles of the octagonal Ammann-Beenker tiling are a rhomb and a square, as depicted in fig. 4.7**a,b)**. A typical local arrangement of the particles is a ring, as depicted in fig. 4.7**c)**. The rhomb exhibits angles of 45° and 135°. However, due to the calculation of the angular distribution we measure $135°/2 = 67.5°$ instead of 135°. The length scales of the Ammann-Beenker tiling are $l_0 = 2\sin\left(\frac{\pi}{8}\right) \approx 0.77$ and $l_1 = 1$. In the following section we choose a temperature of $T = 0.3$ and an exponent $n = 3$. Again, we apply V_A^{ext} with $\zeta = 0$ as angular modification factor.

4.4.1 Supporting the short length scale

In the following, we discuss the results when applying a potential that supports the short length scale of the quasicrystal, i.e. $r_0 = l_0 \approx 0.77$. A typical final structure is a simple square lattice as shown in fig. 4.8. The pair correlation $g(r)$ shows the high positional order of the structure. Furthermore, the angular distribution shows one narrow peak at 90°. Note that using an octagonal quasicrystal as initial configuration of the MC algorithm also leads to a square structure. Thus, we were not able to stabilize the Ammann-Beenker tiling while supporting the short length scale. Instead, we observe a square lattice. The average energy per particle of the ideal Ammann-Beenker tiling is $\langle E/N \rangle \approx -9.6$, whereas the square structure illustrated in fig. 4.8 has an average energy per particle of $\langle E/N \rangle \approx -11.6$. Thus, in case of particles exhibiting eight patches it is probably not possible to stabilize an octagonal quasicrystal by supporting the short length scale.

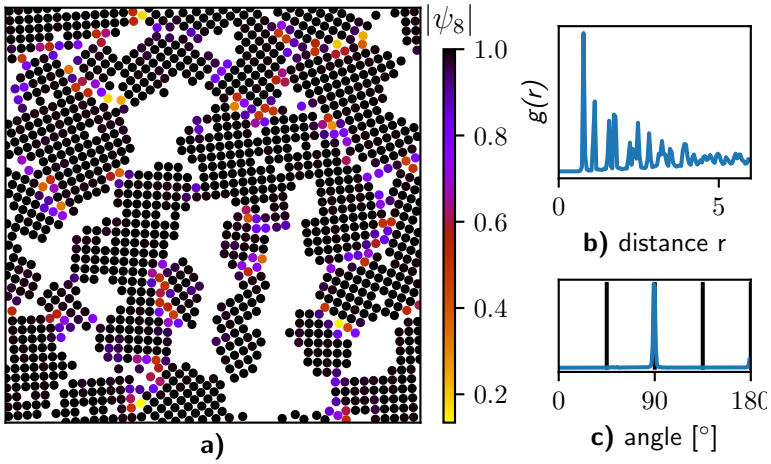

Figure 4.8: **a)** We depict a final particle configuration obtained at $T = 0.3$ and $N = 1393$, using a random initial configuration. The color code illustrates the bond orientational order parameter $|\psi_8|$. **b)** shows the according pair correlation function $g(r)$. Furthermore, we depict the according angular distribution function in **c)**. The black lines indicate angles suitable to octagonal symmetry, i.e. angles of $\{i \cdot 2\pi/8,\ i \in \mathbb{N}\} = \{45°, 90°, 135°, ...\}$.

4.4.2 Supporting the long length scale

Here we choose the minimum of our pair potential at $r_0 = l_1 = 1$. Thus, the shorter length scale l_0 can occur if there is sufficiently high pressure on the system. Again we perform MC simulations with different initial configurations, i.e. the Ammann-Beenker tiling, a square tiling, a zigzag tiling and a random configuration. The so-called zigzag structure is depicted in fig. 4.9. It is a

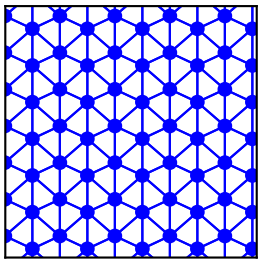

Figure 4.9: Depiction of an ideal zigzag structure. Nearest neighbour particles are connected by lines.

periodic lattice that consists of the same rhombs as the ideal Ammann-Beenker tiling, i.e. it supports angles of 45° and 67.5° = 135°/2. Fig. 4.10 depicts typical final structures where the octagonal quasicrystal and respectively the

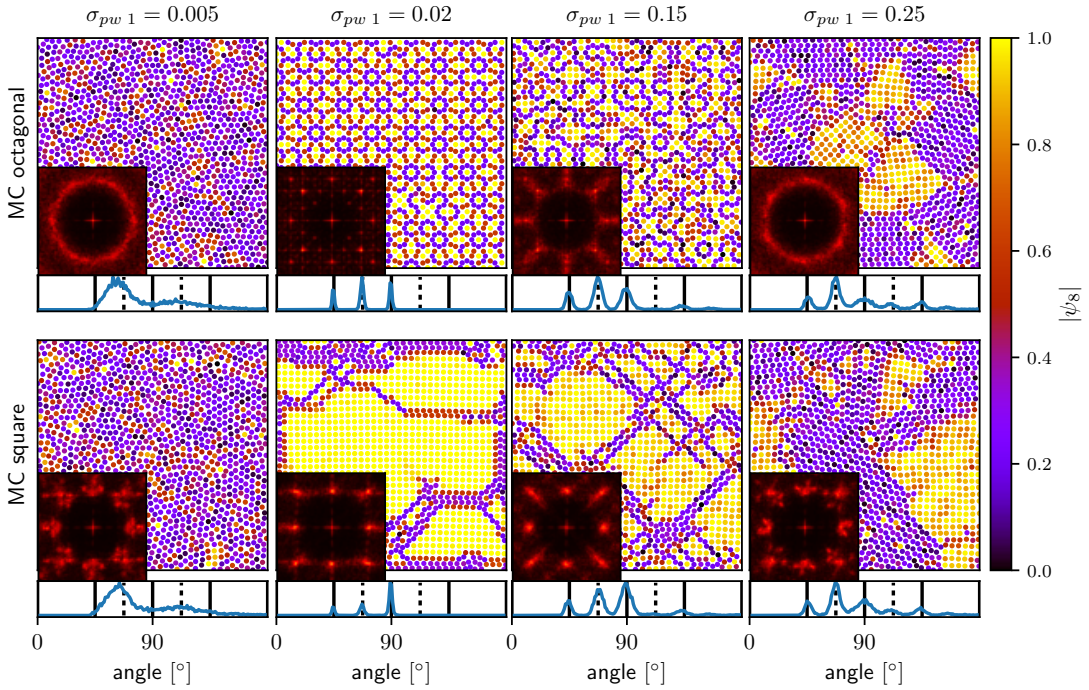

Figure 4.10: Configurations obtained after $5E8$ MC steps with an initial Ammann-Beenker tiling (upper row) and an initial square configuration (lower row) for different patch widths $\sigma_{pw\,1}$ (columns). The insets depict the according structure factor. The graphs below the configurations show the according angular distribution functions. The black lines serve as guide to the eye to indicate angles suiting to octagonal symmetry, i.e. $\{45°, 90°, 135°, ...\}$. The dashed black lines indicate angles in between, i.e. 67.5° and 112.5°. All simulations were done at $T = 0.3$ and $N = 1393$.

square tiling served as initial structures. All of the initial structures were chosen at approximately the same density as the Ammann-Beenker tiling, i.e. $\rho \approx \rho_8 \approx 1.21$. Thus, the square lattice is quenched, i.e. the distance between the particles is smaller than the equilibrium distance. Consequently parts of the square lattice rearrange into the denser zigzag structure (see fig. 4.10). The larger the patch width σ_{pw1}, the more particles of the square lattice rearrange. At very narrow patches $\sigma_{pw1} = 0.005$ we observe structures with low positional and orientational order. The probability of particles escaping from their energetic minimum depends on the temperature and the curvature of the minimum, as discussed in section 4.3.1. Thus, if the patch width is chosen too small the particles arrange in disordered structures that lack preferred bond angles. The octagonal quasicrystal remains stable for narrow patches $0.005 < \sigma_{pw1} \lesssim 0.1$. The angular distribution shows three narrow peaks at approximately 45°, 67.5° and 90°. All of these peaks occur naturally in the Ammann-Beenker tiling. At intermediate patch widths $\sigma_{pw1} \approx 0.15$ the structure dissolves and competes with squares and elements of the zigzag structure. At high patch widths $\sigma_{pw1} \geq 0.2$ all simulations result in a mixture of square and zigzag structure independently of the initial structure. The reason for this mixture is the density. The zigzag structure has a higher density than the quasicrystal, whereas the density of the ideal square structure is lower than that of the quasicrystal $\rho_{square} < \rho_8 < \rho_{zigzag}$. Thus, in case of large patch widths we observe a coexistence of both structures.

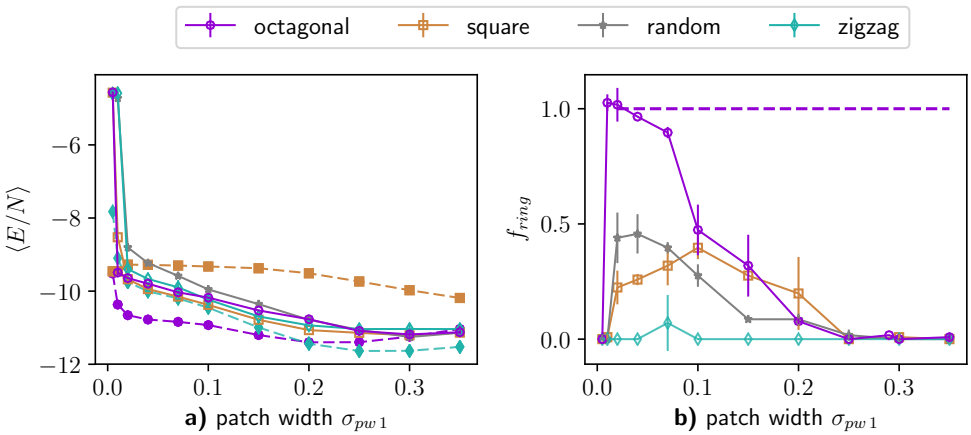

Figure 4.11: **a)** Energy per particle of the ideal structures (filled markers) and accordingly the structures formed after $5E8$ MC steps (hollow markers). **b)** Normalized ring fraction f_{ring} in dependence of the patch width σ_{pw1}. The dashed, purple line highlights the ring fraction of the ideal Ammann-Beenker tiling.

Fig. 4.11**a)** depicts the energy per particle $\langle E/N \rangle$ of the different structures. One can clearly see that the energy of the ideal octagonal quasicrystal is

the lowest for $\sigma_{pw1} \lesssim 0.15$. However, the energy of the final structures is approximately the same for octagonal, square and zigzag initial structure. Thus, at lower temperatures the quasicrystal might be stable. In the case of large patch widths $\sigma_{pw1} > 0.2$ a zigzag structure is energetically preferred. However, due to the higher density the resulting phase is a mixture of square and zigzag structure. $|\psi_8|$ is not a suitable order parameter for distinguishing octagonal and square tiling. Therefore, we choose the normalized ring fraction $f_{ring} = N_{ring}/N/f'_{ring,8}$ where N_{ring} denotes the number of rings and $f'_{ring,8}$ denotes the ring fraction of the ideal octagonal quasicrystal. In this context a ring is identified by its central particle, which has at least seven neighbours at a distance $d < 1.05$. Thus, fig. 4.11**b)** depicts a quantitative measure of local octagonal order. Structures formed with an octagonal quasicrystal as initial configuration show very high ring fractions $f_{ring} > 0.89$ at low patch widths $\sigma_{pw1} \leq 0.07$. Moreover, both square and random initial configuration result in structures that have some local octagonal arrangements $0.2 < f_{ring} < 0.5$ for $\sigma_{pw1} \leq 0.2$. Lastly, at patch width $\sigma_{pw1} = 0.35$ the particles approach the form of isotropic particles. The resulting structures exhibit larger six-fold orientational order with a bond orientational parameter of $\langle|\psi_6|\rangle \approx 0.75$.

4.5 Conclusion

We have investigated a model of patchy particles using a Metropolis algorithm. Our aim was to find decagonal and octagonal quasicrystals. We used different initial structures in order to find the most likely stable structure and examined the resulting structures in dependence of the patch width σ_{pw1}.

In the case of particles exhibiting ten patches we find a metastable decagonal quasicrystal at narrow patch widths when supporting the short length scale of the according quasicrystal $r_0 = l_0$. However, this decagonal quasicrystal is only metastable, as there is a denser phase of lower energy. At larger patch widths we find the stable phase to be a periodic phase that does not support angles suiting to decagonal symmetry. By supporting the long length scale of the quasicrystal $r_0 = l_1$ we find an amorphous structure that exhibits high decagonal order at a narrow patch width, i.e. $\sigma_{pw1} = 0.03$.

In the case of particles exhibiting eight patches we observe square lattices by supporting the short length scale of the octagonal quasicrystal $r_0 = l_0$. By supporting the long length scale of the octagonal quasicrystal we can stabilize the quasicrystal at narrow patch widths. However, the final structures depend strongly on the initial structure. The mixture of square and zigzag structure has about the same energy per particle as the final quasicrystal at $T = 0.3$. At narrow patch widths the ideal quasicrystal has the lowest energy of the tested structures. Thus, it might be stable at lower temperatures. Furthermore, we observe local octagonal arrangements when starting the algorithm with random

configurations at narrow patch widths.

In summary, we found metastable decagonal and octagonal quasicrystals using particles of the desired rotational symmetry, i.e. ten and respectively eight patches with patch widths of $0.005 < \sigma_{pw1} \lesssim 0.1$. Note that the choice of the equilibrium distance, i.e. the position of the potential minimum, is important. While supporting short length scale of the quasicrystal $r_0 = l_0$, the long length scale l_1 has to be supported solely by the energy gain induced by the patches. While supporting the long length scale $r_0 = l_1$, the short length scale may additionally be supported by sufficient pressure on the system. We have shown that both approaches can lead to metastable quasicrystals. In case of the decagonal quasicrystal the difference between the length scales is larger than it is for the octagonal quasicrystal. This might explain why particles exhibiting ten patches form structures of low positional order whereas particles exhibiting eight patches form a quasicrystal when the long length scale is supported in both cases. In contrast, the dodecagonal square-triangle tiling can be formed by particles exhibiting five patches with a width of $\sigma_{pw} = 0.49$. These are particles, that neither exhibit twelve-fold symmetry nor support the bond angles of the tiling, i.e. 60° and 90°. It is even more astonishing that these particles clearly form a stable dodecagonal quasicrystal.

5 Growth of dodecagonal quasicrystals

In teamwork with Miriam Martinsons we study differences between the growth of dodecagonal quasicrystals with particles interacting according to an isotropic pair potential and particles interacting due to the pair potential with preferred bond angles, as introduced in section 3.1. We will now introduce the pair potential used for simulating isotropic particles.

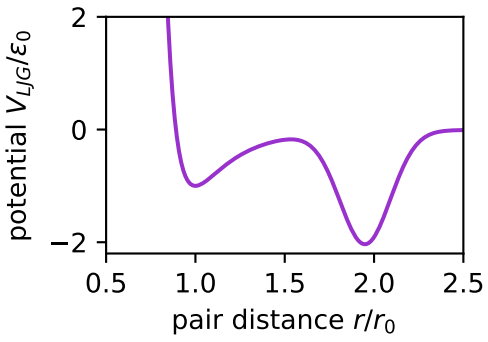

Figure 5.1: Isotropic Lennard-Jones-Gauss pair potential, that stabilizes dodecagonal quasicrystals.

The isotropic pair potential is called the Lennard-Jones-Gauss potential and reads

$$\frac{V_{LJG}}{\epsilon_0} = \frac{V_{LJ}(r)}{\epsilon_0} - \epsilon \exp\left(-\frac{(r-r_G)^2}{2r_0^2\sigma^2}\right). \tag{5.1}$$

We choose the potential parameters as $r_G = 1.95$, $r_0 = 1$, $\epsilon = 2.0$ and $\sigma^2 = 0.02$. Position, depth and width of the second minimum are determined by the parameters r_G, ϵ and σ^2. Fig. 5.1 depicts the Lennard-Jones-Gauss potential. In case of the patchy particles, we use particles with five regularly arranged patches. We apply the pair potential as given in eq. 3.1, choosing the parameters as $\sigma_{pw} = 0.49$ and $r_0 = 1$. Thus, both regarded systems support the same (short) length scale.

5.1 Method

Here, the growth is modelled at a solid-gas interface. All particles within our simulations underlie Brownian dynamics - as described in section 3.3. Figure 5.2 depicts the schematic setup of our simulation. At the bottom of the simulation box are initial layers of an ideal quasicrystal. The lowest layers (coloured in black) are fixed such that the growing crystal is anchored to the box at y=0. Periodic boundary conditions are applied in x-direction. In order to reduce the computational effort, the gas is not simulated as such. Instead, the gas

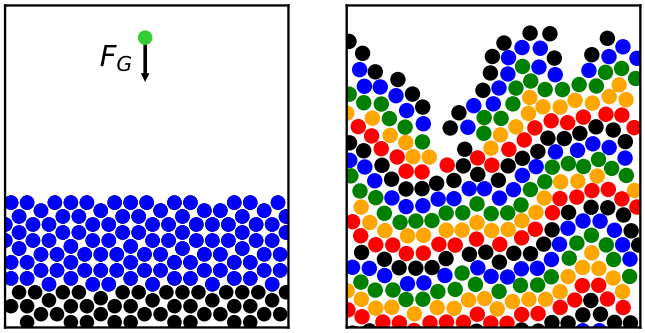

Figure 5.2: **a)** Schematic setup of the simulation. Initial ground ground particles forming an ideal quasicrystal lie at the bottom of the box. Black particles are fixed, while blue particles follow Brownian dynamics. **b)** Schematic depiction of the layers in a grown system.

particles are added at the top of the box and driven downwards, i.e. in negative y-direction with an additional gravitation-like force $\mathbf{F}_G$. As soon as a particle reaches the surface, i.e. its distance to a particle belonging to the ground particles is smaller than 1.24, we turn off $\mathbf{F}_G$ and count the particle as ground particle. The sedimentation rate R describes how many particles are added to the system within one τ_B.

In order to analyse our systems quantitatively we apply the same method as described in [24], i.e. the systems are divided into different layers according to the distance of a particle from the surface. Fig. 5.2**b)** exemplarily depicts the layers of a grown system. All particles belonging to the surface are identified by a large Voronoi volume $v \geq 1.9$ and belong to the first layer, i.e. the surface layer of the system. Particles with a distance of $d < 1.2$ to a surface particle belong to the second layer. Subsequent layers are determined analogously. Note that d is chosen larger than the short length scale and smaller, than the diagonal of the square tiles $1 < d < \sqrt{2}$.

The following sections (5.2 and 5.3) are taken from our paper *Growth of two-dimensional dodecagonal colloidal quasicrystals: Particles with isotropic pair interaction with two length scales vs. patchy colloids with preferred binding angles* in the version that was submitted to *Eur. Phys. J. E* on 9/18/2018. All simulations regarding isotropic particles were done by M. Martinsons, all simulations regarding patchy particles were done by A. Gemeinhardt.

5.2 Results

In this section we show and compare the results of our simulations. First, we discuss diffusion-limited aggregation that occurs at low temperatures. Second, we present the structures grown with different control parameters and characterize them according to the occurrence of the long length scale. Third, we determine the bond-orientational and positional order for the grown quasicrystalline structures. Fourth, we describe the dynamics of the particles with a special emphasis on phasonic flips and particles at the surface. Finally, we explore the consequences of the observed lines or regions with phasonic flips in order to find out how perfect the grown quasicrystals are.

5.2.1 Diffusion-limited aggregation

First, we consider extreme examples of very low temperatures, for which the diffusion of particles along the surface of a grown structure is very small. Figures 5.3 (a,b) show two typical snapshots of systems grown with $R = 2/\tau_B$ and (a) $T = 0.001$ for particles interacting according to the isotropic potential and (b) $T = 0.00001$ in the case of the potential with preferred bond angles. In both cases we find network-like structures as expected for diffusion-limited aggregation (cf. [48]), *i.e.* the diffusion time for a particle to find its ideal position is smaller than the time between two injected particles.

In the case of the isotropic system, we observe thin branches composed of particles for which the nearest neighbor distance corresponds to the long length scale of the interaction potential. The preference of the long length scale is due to the fact that newly injected particles first get stuck at the surface with this long distance to their neighbors and the temperature is too low for the particles to escape from the corresponding minimum of the interaction potential. At a few places the particles build local triangular arrangements.

In the case of the system with preferred binding angles, we also observe the formation of network-like structures. Naturally, we only observe the short length scale between neighboring particles in these systems, as this is the only length supported by the potential. Unlike the isotropic system, the patchy particles form thicker branches with triangular and square tiles corresponding to local dodecagonal arrangements.

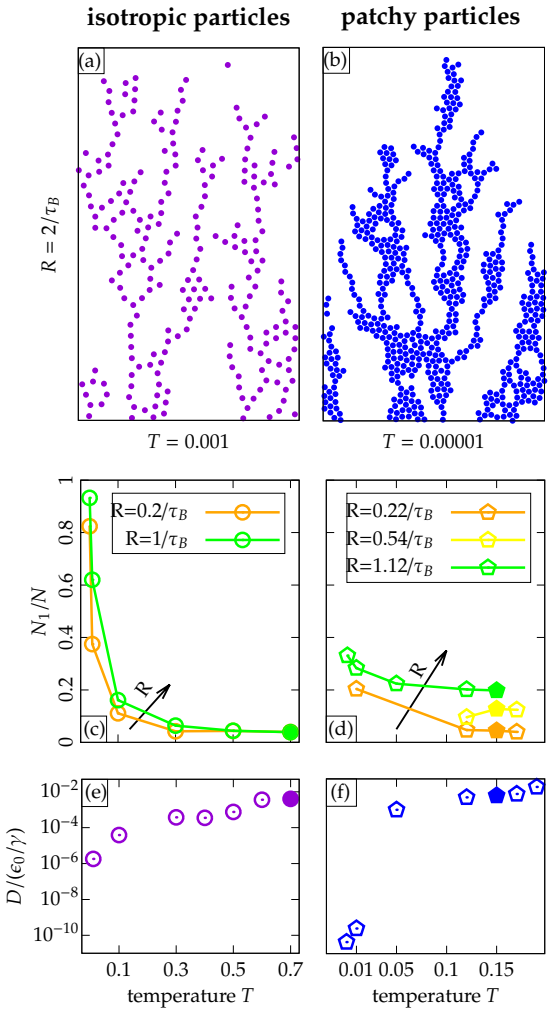

Figure 5.3: Network-like structures grown at very low temperatures, *i.e.* diffusion-limited aggregation with isotropic and patchy particles on the left and right hand side, respectively. The initially perfectly ordered substrate particles are not shown. (a) Isotropic particles arrange to thin branches with the distance between neighboring particles given by the long length scale of the interaction potential. (b) Patchy particles form thicker branches with local dodecagonal order. (c,d) illustrate the fraction of surface particles as a function of the temperature. Different rates are depicted in different colors. (e,f) show the diffusion constants of a particle on a free surface dependent on the temperature. Systems grown with our standard temperatures $T = 0.70$ or $T = 0.15$ for isotropic or patchy particles, respectively, are marked by filled symbols.

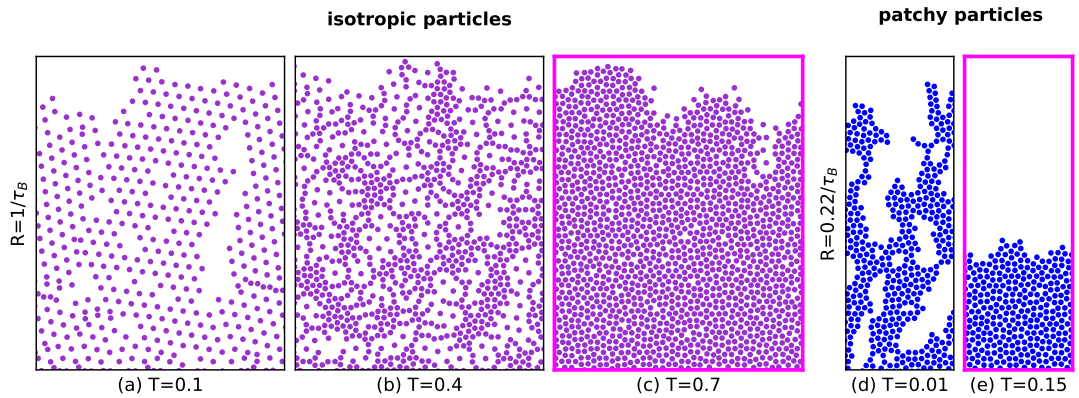

Figure 5.4: Exemplary snapshots of systems with isotropic and directed interactions for different temperatures. (a-c) show isotropic systems grown with $R = 1/\tau_B$ and (a) $T = 0.1$, (b) $T = 0.4$ and (c) $T = 0.7$. (d-e) illustrate systems of patchy particles grown with $R = 0.22/\tau_B$ and (d) $T = 0.01$ and (e) $T = 0.15$.

Figures 5.3 (c,d) quantify the grown structures by illustrating the fraction of particles in the surface layer over the total number of particles as a function of the temperature for (c) isotropic and (d) patchy particles. Note, due to the different types (and energies) of the interaction, it is hard to compare the temperature of a quasicrystalline structure observed for isotropic interactions to the temperature for which a quasicrystal with patchy colloids is found. However, we choose a reference temperature for each of the systems where the resulting quasicrystals are comparable. To be precise, for $T = 0.70$ in case of isotropic interactions and $T = 0.15$ in case of directed interactions we obtain nicely grown quasicrystals that for similar rates are comparable concerning the orientational order (see sec. 5.2.3) and the averaged number of flips (see sec. 5.2.4) within the systems. *I.e.* in isotropic systems with $T = 0.70$ the averaged bond-orientational order parameter in layers deeper than six reads $\langle|\psi_{12}|\rangle = 0.724...$ and the averaged number of flips is $N_{flip}/N = 0.048...$, which is similar to systems with directed interactions and $T = 0.15$ in which $\langle|\psi_{12}|\rangle = 0.728...$ and $N_{flip}/N = 0.061....$ Accordingly, in the following we refer to the temperatures mentioned above as standard temperatures and data for systems grown with these temperatures are shown with solid points or thicker lines in all figures of this articles. Furthermore, snapshots of the systems grown with our standard temperatures are usually emphasized by a frame colored in magenta.

The results of fig. 5.3 (c,d) show that with increasing temperature the number of surface particles decreases indicating that for larger temperatures no network-like structures occur. Different colors of the data points represent systems grown with different rates.

In the case of the isotropic particles, we observe quasicrystalline bulk structures in the temperature regime $T \in [0.5, 0.7]$. Here, the fraction of surface particles does not significantly depend on the rate. For lower temperatures the fraction of surface particles is larger for systems grown with higher rates since a reduced time between injected particles causes gaps and respectively increasingly thinner branches. In the case of the patchy particles, the fraction of surface particles also rises at low temperatures due to the formation of network-like structures. However, the branches of the structures built in these systems are thicker, such that the fraction of surface particles is lower than for the corresponding cases in the isotropic systems. Furthermore, the network-like structures are still observable for larger temperatures, especially in case of large rates. Even at larger temperatures the fraction of surface particles depends on the rate in case of patchy colloids. At high temperatures $T \geq 0.15$, this is due to increased cluster formation, which will be discussed in sect. 5.2.4. In conclusion, while for isotropic interactions the dependence of the surface particles on the rate is small in case of large temperatures, in case of patchy colloids, the rate even matters at larger temperatures and in order to avoid diffusion-limited aggregation a low injection rate is required.

Additionally, in order to give a quantitative estimate of the diffusion of the particles on the surface dependent on the temperature, we extract the diffusion constant D from the mean square displacement of single particles on a free surface (see figure 5.3 (e,f)). For both, isotropic and patchy particles, D increases with temperature and covers several orders of magnitude within the investigated temperature ranges. Low diffusion constants explain the formation of networks, while increased D allow wide diffusion and the growth of quasicrystals. Note that the diffusion constants of patchy colloids on average are larger than for particles with isotropic interactions at comparable temperatures, because they usually do not bind with a patch to the surface during the diffusion along the surface. As soon as a patchy colloid connects to the surface by a patch it stays at that position much longer than an isotropic particle.

5.2.2 Overview of the observed structures and the occurrence of the long length scale

In the next step, we want to explore at which temperatures quasicrystals can be grown. Figure 5.4 qualitatively depicts typical snapshots of systems obtained from both studied potentials for different temperatures. In fig. 5.4 (a-c) we illustrate systems with isotropic interactions grown with a constant rate $R = 1/\tau_B$. We observe two structures where the long length scale dominates and an almost perfect quasicrystal. By almost perfect quasicrystal we mean that most of the particles sit at the positions that are expected from the perfect square-triangle tiling that we employ as a substrate. A quantitative characterization of possible deviations from a perfect square-triangle tiling will be given starting

in sect. 5.2.3. While we usually compare the positions of the particles of the grown structure to that of the square-triangle tiling in real space, one can also check the long-range order by calculating the structure factor as we will show in sect. 5.2.3.

In our systems grown with $T = 0.10$ (see fig. 5.4 (a)) the particles arrange to local triangular structures with nearly exclusively particle distances of the long length scale. Only a few particles reach the first potential minimum of the short length. The structure is interrupted by gaps due to a reduced diffusion at low temperatures. Increased temperatures result in an increased local dodecagonal ordering, which is illustrated on the example of a system grown with $T = 0.40$ in fig. 5.4 (b). A striking feature here is the formation of rings or parts thereof, which are composed of a central particle that is surrounded by twelve colloids. The distance of the central particle to the outer particles corresponds to the long potential length while the distances between the surrounding particles is the short length. For even larger temperatures the number of rings decreases and finally the denser, almost perfect quasicrystalline structures grow (*e.g.* fig. 5.4 (c) for $T = 0.70$).

In fig. 5.4 (d-e) structures grown with patchy particles are shown. The snapshots illustrate systems grown with $R = 0.22/\tau_B$. Even for very low temperatures (*e.g.* $T = 0.01$, fig. 5.4 (d)) we do not observe a domination of the long length scale. Instead, the discussed network-like structure is present over a wide temperature range. With rising temperature the networks become thicker until quasicrystalline structures grow for sufficiently large temperatures as depicted for $T = 0.15$ in fig. 5.4 (e).

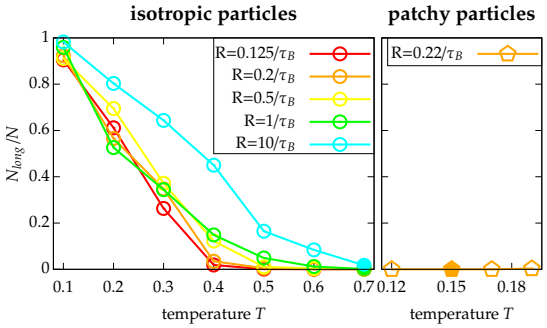

Figure 5.5: Fraction of particles for which all distances to neighboring particles except at most one correspond to the long length scale as a function of the temperature. Different rates are shown with different colors and the standard temperatures are marked by filled symbols. Systems grown with isotropic interactions are shown on the left hand side, patchy particle systems on the right hand side.

In fig. 5.5 we characterize the occurrence of the long length scale quantitatively. As a function of the temperature, we show the fraction of particles

that possess - except for at most one neighbor - only neighbors at a distance corresponding to the long length scale. Such particles are either part of a local triangular arrangement with the long length or they are the central particle of a ring-like formation. The initial particles of the substrate and the surface particles are not included in the evaluation. Particles with a distance $d < 1.6$ are defined as nearest neighbors with the short distance, while particles with $1.6 < d < 2.2$ are counted as nearest neighbors with the long distance. For each temperature we consider systems grown with various rates as given by the color code.

For isotropic particles the long length scale dominates for low temperatures. Furthermore, increasing the rates seems to support the long length scale. For $T = 0.10$ and $R = 10/\tau_B$ nearly all particles exclusively have distances of the long length to their neighbors. For sufficiently large temperatures we observe the formation of quasicrystalline structures, *e.g.* for $T = 0.70$ we observe hardly any particles with only neighbors of the long length for any rate. In systems grown with patchy particles we do not observe any particles that possess only neighbors with the long length distance which is shown on the example of one representative rate.

5.2.3 Order of the grown quasicrystalline structures

In the following, we concentrate on the almost perfectly grown quasicrystalline structures, *i.e.* the structures grown with or close to our standard temperatures which are sufficiently large. Furthermore, we consider sedimentation rates that are sufficiently low.

We characterize the structures according to their bond-orientational as well as positional order (see fig. 5.6). Therefore, we calculate the bond-orientational order parameter $\psi_m(\boldsymbol{r}_j) = 1/N_k \sum_{k=1}^{N_k} \exp(\mathrm{i}m\theta_{jk})$ for each particle j at position $\boldsymbol{r}_j$. The sum includes all neighboring particles $k = 1, ..., N_k$ with a distance of the short length scale. We determine the bonds of such neighbors to the considered particle j. The angles between such bonds and an arbitrary fixed reference axis are denoted θ_{jk}. m gives the symmetry of the bonds which for testings of dodecagonal order is chosen $m = 12$. In fig. 5.6 (a,b) we depict exemplary snapshots of systems grown with our standard temperature and give the absolute value of the local bond orientational order parameter by the colors. Most particles show a good local dodecagonal order indicated by the black color. Slight deviations are caused by thermal fluctuations. In addition, in fig. 5.6 (c,d) we depict the corresponding structure factors $S(\boldsymbol{q}) = 1/N \sum_{i=0}^{N-1} \sum_{j=0}^{N-1} \exp[2\pi\mathrm{i}\boldsymbol{q}(\boldsymbol{r}_i - \boldsymbol{r}_j)]$ with wave vectors $\boldsymbol{q}$ and positions of the particles $\boldsymbol{r}_i$. Discrete Bragg peaks indicate long-range order of the structures. Positional order is also indicated by sharp peaks in the radial distribution functions $g(r)$ shown in fig. 6 (e,f). The positions of the peaks correspond to the ones of an ideal square-triangle tiling. Note that the peak at the short

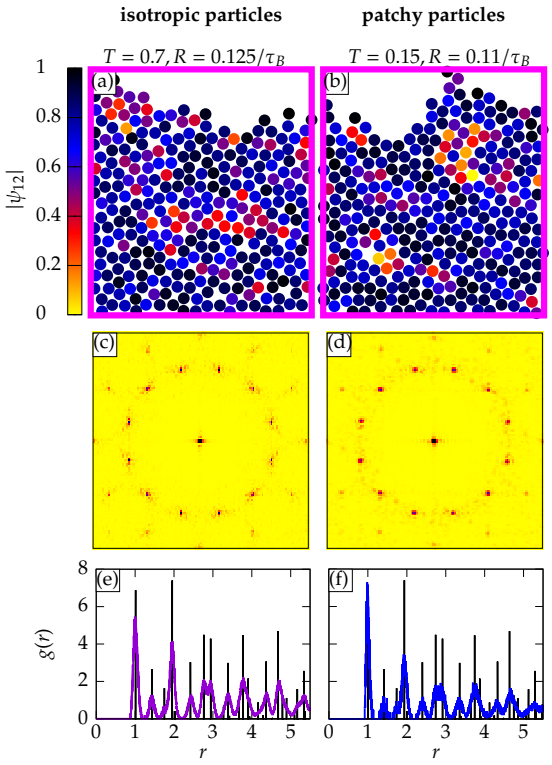

Figure 5.6: Characterization of structures grown with our standard temperatures. The interactions between the particles are isotropic (left column) and with preferred bond angles (right column). (a,b) Snapshots of grown structures with the particles colored according to their absolute value of the bond-orientational order parameter $|\psi_{12}|$. (c,d) Structure factors $S(\boldsymbol{q})$ and (e,f) radial distribution functions $g(r)$ depicted in purple or blue of the illustrated snapshots. The radial distribution function of an ideal square-triangle tiling is shown in black for comparison. Note that $g(r)$ of the ideal tiling is compressed by a factor of 70 in y-direction.

length scale is larger and thinner in the case of interactions with preferred angles. All in all, at the respective standard temperatures the structures grown with isotropic interactions and the structures for interactions with preferred bond angles are almost the same and they correspond to nearly perfect square-triangle tilings as can be revealed by comparing the positions of the particles in real space (see also quantitative analyses in the next section).

In fig. 5.7 we quantitatively show the orientational order as a function of the layers for systems grown with different control parameters that support quasicrystalline structures. The left column illustrates isotropic particles; in the right column we depict patchy particles. Figures 5.7 (a,b) show the orientational order for systems grown with our standard temperature $T = 0.70$ for isotropic

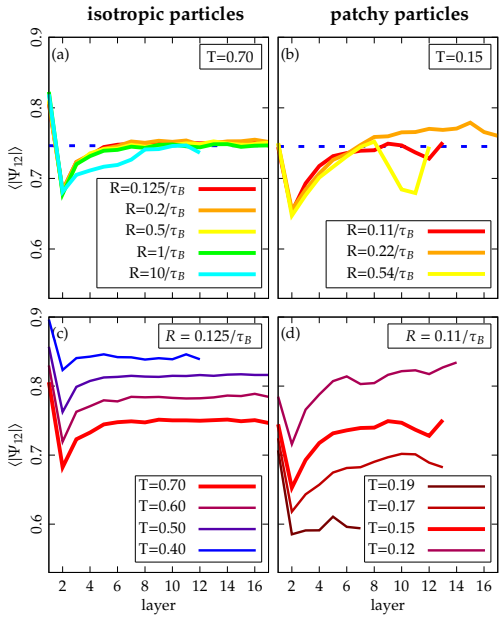

Figure 5.7: Averaged bond-orientational order parameters $\langle|\psi_{12}|\rangle$ as functions of the layer in systems with isotropic particles (left column) and for patchy particles (right column). The bond-orientational order for our standard temperatures ($T = 0.70$ for isotropic interactions, $T = 0.15$ for patchy colloids) is indicated by thick curves. In (c,d) the temperatures are varied for constant rates ($R = 0.125/\tau_B$ for isotropic interactions, $R = 0.11/\tau_B$ for patchy colloids). The dotted lines indicate the reference values of $\langle|\psi_{12}|\rangle$ obtained when the respective system is equilibrated in bulk with the respective standard temperature. The layers are counted starting at the surface, which corresponds to layer one.

particles and $T = 0.15$ for patchy particles. These temperatures are comparable regarding the averaged value of $|\psi_{12}|$ (shown by the blue dotted lines) in a system equilibrated at the corresponding temperature.

For all rates the orientational order possesses a large value in the first layer, which is due to several surface particles with only one nearest neighbor. Starting from the second layer, the system first is less ordered but the order increases with increasing distance from the surface. Finally, the orientational order parameter approaches the bulk reference value after about six layers. The orientational order usually is independent of the rate. However, for very high rates, as shown on the example of $R = 10/\tau_B$ for isotropic particles, the increase of the order is slower and it takes more layers to approach the bulk value because the injected particles have less time to find their ideal positions. The behavior of the bond orientational order at the standard temperatures is similar for isotropic interactions and patchy colloids.

In fig. 5.7 (c,d) we display the course of the order in systems grown with a constant rate, *i.e.* $R = 0.125/\tau_B$ for isotropic particles and $R = 0.11/\tau_B$ for patchy particles. The temperatures are varied. In all systems the orientational order is largest for low temperatures since thermal fluctuations are reduced.

5.2.4 Dynamics of phasonic excitations

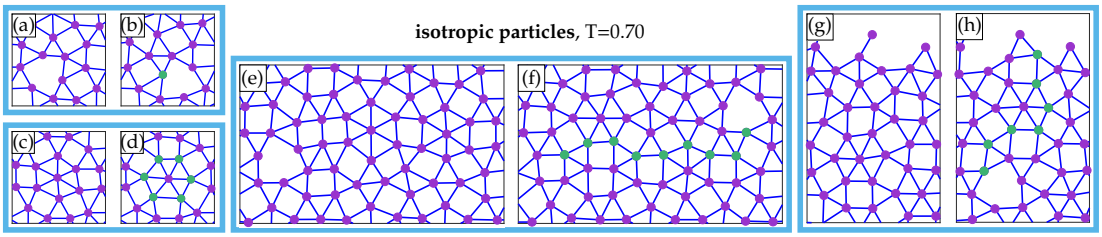

Figure 5.8: Local rearrangements during the dynamical evolution of a system with isotropic interactions and standard temperature. In each blue box a part of the system is shown at two different times. Particles that have changed their position about d_{flip} are colored in green. A tiling is drawn by connecting the particles with a distance of the short length. (a,b) Single flip enabled by a shield tile. (c,d) Correlated flips of a ring of six particles rotating around a central particle. (e,f) Successive flips starting from a shield tile in the bulk and leading to a displacement of the shield tile. (g,h) Successive flips starting at the surface and leading to a shield tile that moves into the bulk. Similar dynamics are also observed in systems of patchy particles.

Within our grown systems there might still occur rearrangements of the particles: Beside thermal phononic fluctuations, phasonic flips play an important role in the discussion of the dynamics. In the well-studied decagonal tiling local phasonic flips of single particles have been observed at many positions in the tiling [13–15, 18, 24]. We will now discuss the case of dodecagonal quasicrystals in which we observe two kinds of flips which occur for both, systems with isotropic interactions as well as interactions with preferred binding angles.

First, even though in a local arrangement composed of only squares and triangles the particles are so dense that they do not have the possibility of flipping independently from each other, we observe correlated flips of six particles that rotate about $2\pi/12$ around a central particle as shown in fig. 5.8 (c,d). The covered distance of each particle corresponds to the flip distance d_{flip}. The ideal flip distance reads $d_{flip} = 1/(2\cos(\pi/12))$, calculated from geometrical considerations.

Second, beside the triangles and squares known from the square-triangle tiling, our grown structures exhibit shield tiles which are additional tiles com-

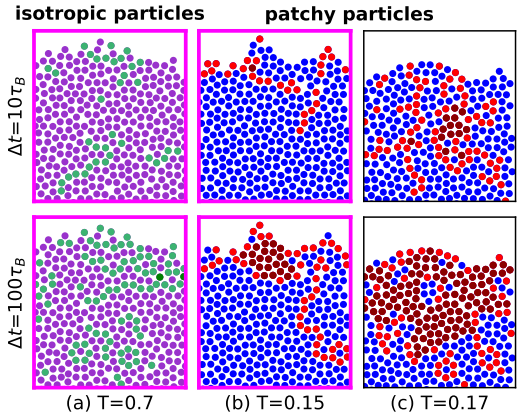

Figure 5.9: Phasonic flips in systems grown with our standard temperatures (a) $R = 0.2/\tau_B$ for isotropic particles and (b) $R = 0.22/\tau_B$ for patchy particles. (c) depicts an additional system of patchy particles grown with a larger temperature $T = 0.17$. Particles that will flip after $\Delta t = 10\tau_B$ (first row) or $\Delta t = 100\tau_B$ (second row) are colored in green or red. Particles that belong to a region that collectively rearranges are colored in dark-green or dark-red.

posed of six particles as illustrated, *e.g.* in fig. 5.8 (a,b). Such shield tiles serve as starting points of phasonic flips (cf. [30,44]), since particles on the sides of a shield may flip inside the shield (see fig. 5.8 (a,b)). The covered distance after a flip is also d_{flip}. After such a flip the shield tile is conserved and only changes its position within the sample. As a consequence, we observe chains of flipping particles (see, *e.g.* fig. 5.8 (e,f)) corresponding to the motion that is known as zipper motion [30,44]. Once one particle has flipped the subsequent flip of the zipper motion may occur very fast, *e.g.* the time between the two illustrated snapshots is only $\Delta t = 1\tau_B$.

In addition, during the growth process new shield tiles may build at the free surface of the quasicrystal and move into the structure by subsequent flips as illustrated in fig. 5.8 (g,h). Conversely, shield tiles within the bulk may also move to the surface and disappear. Note that the examples in fig. 5.8 are drawn for isotropic interactions but similar flipping dynamics also occur in systems of patchy particles.

In the following we show grown systems of isotropic and patchy particles and compare them with regard to phasonic flips. In fig. 5.9 we illustrate snapshots of systems grown with our standard temperatures. The isotropic systems are shown in the first column, patchy systems in the second column. An additional system of patchy particles grown with the slightly larger temperature of $T = 0.17$ is depicted in the third column. The particles are colored according to performed flips after $\Delta t = 10\tau_B$ and $\Delta t = 100\tau_B$ in the first and second line, respectively. We consider a particle to be flipped if it has moved by more than

$d_{flip}/2$ after the considered time Δt. Flipped particles are colored in green or red. Dark-green and dark-red particles possess at least four flipped neighbors. Those particles typically belong to a region where all particles have moved, which we also refer to as rearranged regions. However, note that there might be some particles detected as rearranged regions, although there is only a crossing of flipped lines. Nonetheless, we chose four neighbors or more as threshold, in order to detect all regions.

In all snapshots we observe the flips discussed in fig. 5.8. As expected, by trend the number of flips is larger in case of a longer time between the snapshots since there is more time for the flips to occur. Furthermore, there are more flipped particles close to the surface than in the bulk. In systems with isotropic interactions we hardly observe any regions of collectively rearranged particles. In systems of patchy particles, we observe regions that have rearranged. A quantitative analysis will be given in the next paragraph and fig. 5.11. Such regions even become larger if the temperature is slightly increased and usually occur close to the surface. A possible reason might be that patchy particles need a longer time to orient correctly.

In order to discuss the phasonic flips quantitatively, we show the average fraction of flipped particles in a growing system after a simulation time $\Delta t = 10\tau_B$ as a function of the layer in fig. 5.10. The shown systems are the same as in fig. 5.7. In all systems the fraction of flipped particles is largest close to the surface where particles still need to find their ideal positions. Moreover, in the upper layers we observe slightly more flips in systems of patchy particles compared to isotropic particles. The flip fraction decreases with an increasing distance from the surface. Figures 5.10 (a,b) depict the functions for various rates and our standard temperatures. For systems grown with low sedimentation rates the flip fraction decreases fastest since the particles have the most time to find their ideal positions. Far away from the surface, the fraction of flipped particles approaches the bulk value (dotted blue lines) that is determined by counting the flips in structures equilibrated at the corresponding standard temperatures in bulk. Figures 5.10 (c,d) show the fraction of flipped particles for systems with a constant rate for various temperatures. We observe a pronounced temperature dependence, *i.e.* for large temperatures there are more phasonic flips even at large distances from the surface.

In the following we investigate the rearranged regions quantitatively. Figure 5.11 depicts the fraction of particles belonging to a rearranged region as a function of the rate. The data confirms that the isotropic particles form less rearranged regions, *i.e.* there are hardly any rearranged regions except for a few particles on the surface, which is shown using the example of the largest investigated temperature $T = 0.70$. *E.g.* $N_{region}/N = 0.0028...$ for $R = 0.125/\tau_B$. In case of the patchy systems, the fraction of rearranged regions is much larger and increases with increasing rate for all considered temperatures. Additionally, the fraction of rearranged regions is dependent on the temperature as we have

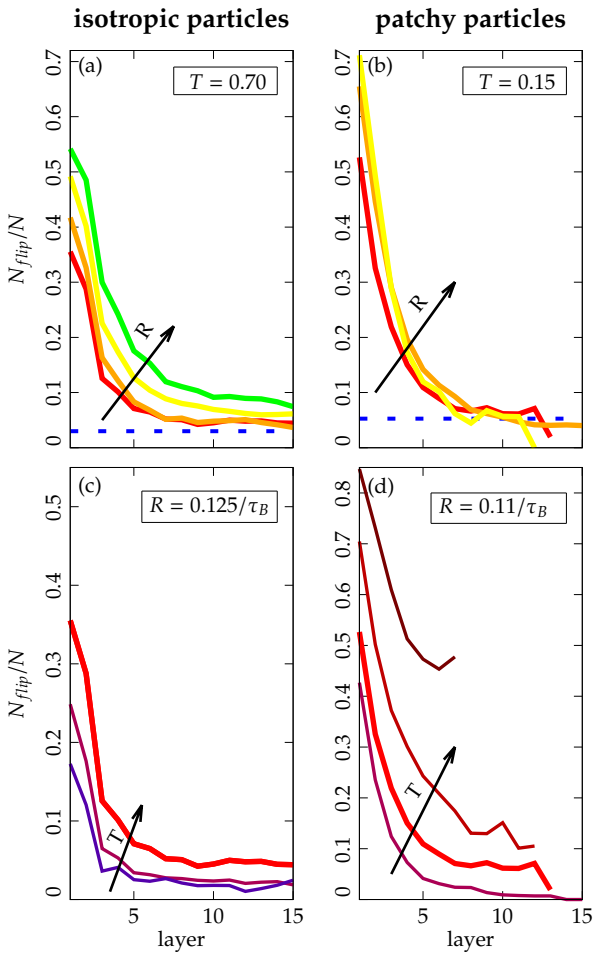

Figure 5.10: Averaged flip fraction after $\Delta t = 10\tau_B$ as functions of the layer. The same systems as in fig. 5.7 are employed. The dotted lines in (a,b) give the reference values of N_{flip}/N obtained from an structure equilibrated in bulk.

already conjectured due to the snapshots shown in fig. 5.9. For example, $N_{region}/N = 0.0253...$ for $T = 0.15$ and $R = 0.11/\tau_B$.

Another kind of dynamics observed during the growth is the dissociation of particles from the surface. Especially within the systems of patchy colloids there are sometimes single particles or chains of particles that detach from the surface. The detached particles subsequently trigger the formation of larger clusters of particles. In fig. 5.12 we show the two different possibilities of how such clusters are formed with time. First, we illustrate the dissociation of a single particle in a system that grows with $T = 0.17$ and $R = 0.54/\tau_B$ (see fig. 5.12 (a-c)). Second, we depict the detachment of a chain of particles that typically occurs at large rates (*e.g.* $R = 1.12/\tau_B$) and not too large temperatures (*e.g.* $T = 0.15$) as shown in fig. 5.12 (d-f). Naturally, the first way of forming

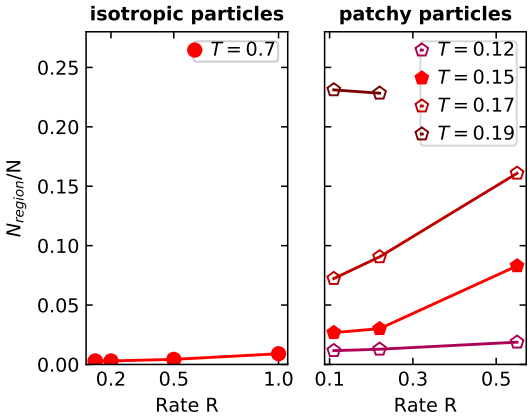

Figure 5.11: Number of particles belonging to a rearranged region after $\Delta t = 10\tau_B$ over the total number of particles within the considered system as a function of the sedimentation rate R. Different temperatures are shown in different colors. The results for isotropic particles are shown on the left, patchy particles on the right.

clusters is observed more often, as it does not require diffusive motion along the surface.

5.2.5 Lines and regions of flipped particles in almost perfect structures

In the following, we investigate how the dynamics of phasonic flips influences the structures that are grown. Specifically, we are interested in deviations from perfect quasicrystals as given by the square-triangle tiling that we have also used for the initial substrate particles. In fig. 5.13 we depict systems that have grown with different sufficiently low sedimentation rates $R \leq 1/\tau_B$ and appropriate temperatures in order to form quasicrystalline structures. The grown structures are illustrated in purple (isotropic particles) or blue (patchy particles) while in the background the perfect square-triangle tiling with particles colored in green or red are shown.

In case of the isotropic interactions (see fig. 5.13 (a-c)) most particles of the grown structures coincide very well with the positions expected from the perfect square-triangle tiling. However, we observe lines of particles that are located between two ideal lattice positions. The deviation from the next ideal position corresponds to the distance of a phasonic flip d_{flip}. Note, we do not observe single particles whose positions deviate from the prescribed ideal positions. To be specific, we observe the rotation by $2\pi/12$ of rings of six particles around a central particle similar to fig. 5.8 (c,d). Furthermore, there arise even longer chains of displaced particles. Such chains are either closed or

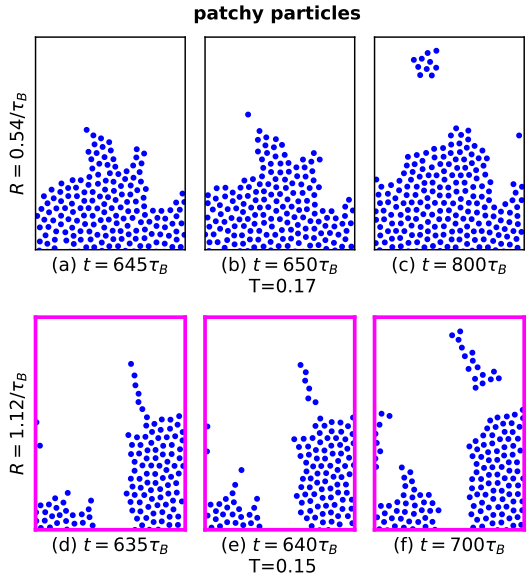

Figure 5.12: Two examples of cluster formation with time. (a-c) depicts a single particle that diffuses from the surface. Particles, that are added to the system attach to it and form a small cluster. (d-f) shows a complete chain of particles that detach from the surface.

open. The endpoints of open chains are either at the surface of the structure or in the bulk. In the latter case they begin with a shield tile. Note that on a first glance the patterns of closed and open lines in figs. 5.13 (a-c) seem to be quite different. However, the patterns of circles and lines can change very fast. In total, we do not find any dependence of the phasonic flip lines on the sedimentation rate for the isotropic interactions. Note that we do not show the complete width L_x such that the patterns are not continued periodically in the snapshots.

In case of the systems grown with preferred binding angles as depicted in figs. 5.13 (d-f), similar circles and lines of flipped particles are observed. However, close to the surface the patchy particles generally do not coincide well with the perfect structure. Even regions of mismatched particles occur probably as a direct consequence of the dynamically rearranging regions that we have observed in sect. 5.2.4. Particles belonging to a rearranged region are colored in light-blue. Hence, we calculated the displacement fraction, *i.e.* the fraction $f_{disp} = N_{disp}/N$ of particles N_{disp} belonging to a displaced region averaged over 1000 snapshots. In case of the patchy systems, we find a displaced particle fraction of $f_{disp} = 20.8\%$ for the system grown with $T = 0.15$ and $R = 0.11/\tau_B$ and $f_{disp} = 36.7\%$ for $R = 0.22/\tau_B$. In contrast, the displaced particle fraction in case of the isotropic particles is only $f_{disp} = 0.9\%$ for $T = 0.70$ and $R = 0.125/\tau_B$ and $f_{disp} = 13.9\%$ for $R = 0.2/\tau_B$. Thus, the displaced particle fraction depends

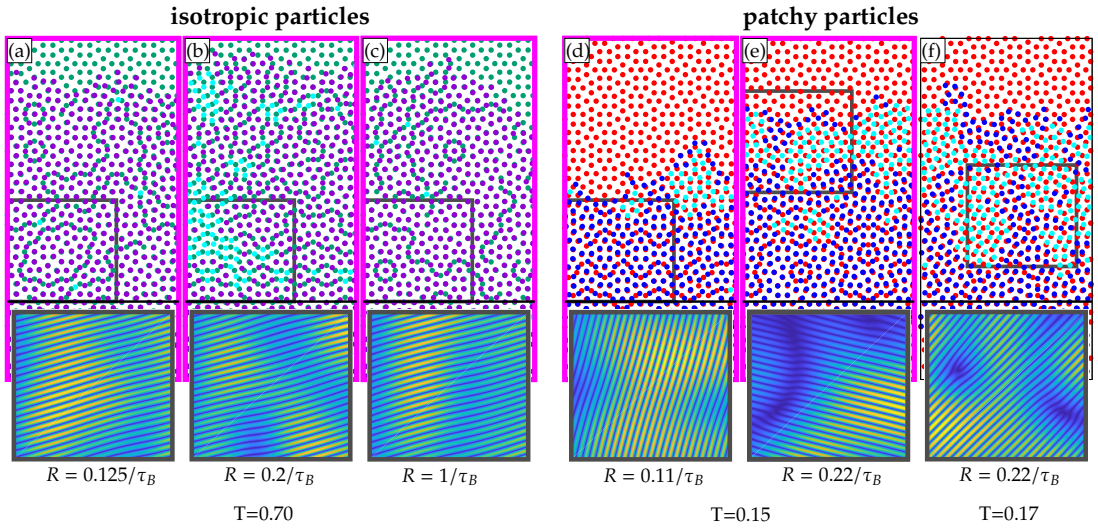

Figure 5.13: Comparison of grown structures (purple or blue points) to quasicrystals according to perfect square-triangle tilings (green or red points). (a-c) depict systems grown with isotropic interactions, (d-f) show particles with preferred binding angles. The rates and temperatures are given in the figure. The border to the initial substrate particles is indicated by black lines. In order to indicate regions with phononic or phasonic offset, particles that are neighbored by particles that all are displaced from the perfect structure are colored in light-blue. The insets show the Fourier back transformations of symmetrically chosen peaks of the structure factor in order to detect dislocations. Within the snapshots of the grown structures we highlight the regions which are illustrated in the insets by gray borders. Note that dislocations only have been found for patchy particles (see insets of (e) and (f)).

on the rate and is much higher for the patchy systems. However, note that in case of lines that lay closely side by side the particles may misleadingly be counted to a rearranged region (see, *e.g.* fig. 5.13 (b)).

Finally, we checked whether dislocations occur in the grown structures. By using the method described in [19], we find that for isotropic interactions no dislocations can be found while in case of patchy colloids dislocations might build, especially in case of large rates or large temperatures (see insets in fig. 5.13). The dislocations seem to form at the border between the almost perfect part of the grown quasicrystal and a region that is collectively displaced with respect to the perfect structure.

5.3 Conclusions

We have investigated the particle-resolved growth of dodecagonal quasicrystals in two dimensions by sequentially depositing particles at a free surface of the growing structure. The method corresponds to the growth out of vapor. To be specific, by employing Brownian dynamics simulations we have studied the growth of quasicrystals consisting of particles that interact according to an isotropic pair potential of the Lennard-Jones–Gauss type or of structures formed by so-called patchy colloids that interact with a Lennard-Jones potential and additionally possess preferred bond angles.

We have analyzed structures grown with different sedimentation rates and temperatures according to their orientational order. While for low temperatures we observe the phenomenon of diffusion-limited aggregation that leads to network-like structures, the best quasicrystals are obtained for large temperatures as long as we stay below the melting transition. With larger temperatures, phasonic flips occur more frequently in the structures. Since the flips close to the surface dominate, these flips support the growth of almost perfect quasicrystals because they enable the healing of structures close to the surface that initially had been flipped in a wrong way. Note that this mechanism can also be observed for the growth of metallic quasicrystals [28].

At intermediate temperatures differences between the structures grown with isotropic particles and those obtained with patchy colloids can be observed. In case of the isotropic particles the long potential length scale dominates for low temperatures. Note that we have made similar observations for the decagonal quasicrystals studied in [24]. In case of the dodecagonal square-triangle quasicrystals considered here, the long length scale leads to triangular arrangements or ring-like defect tiles. In addition, phasonic flips corresponding to zipper motions with additional shield tiles are observed (cf. the theoretical work in [30]).

The growth of quasicrystals that consist of patchy particles is not based on the competition of two given length scales. Therefore, patchy particles have the advantage that the second length scale of the quasicrystal is not supported directly by the pair potential but only indirectly via the preferred binding angles. As a consequence, we do not find defects based on an undesired dominance of the long length scale, *e.g.* the ring structures with long nearest neighbor distances that can be found for isotropic interactions do not occur for patchy colloids. On the downside, for patchy colloids we observe the occurrence of regions with different phononic or phasonic displacements. These regions sometimes are connected to dislocations that have not been observed in case of isotropic particles. The regions with different phasonic displacement and the dislocations are probably due to the smaller mobility at the surface in combination with the requirement to not only adjust the positions to the perfect structure but also the orientation.

In conclusion, patchy particles provide an interesting alternative way to obtain almost perfect soft matter quasicrystals. They also might present an interesting approach concerning the struggle to obtain well-controlled colloidal quasicrystals in experiments. However, some questions remain open for future studies, *e.g.* concerning the mechanism how the second length scale of the quasicrystal is supported by the binding angles and why colloidal particles with five or seven patches form dodecagonal quasicrystals [35,45] instead of structures with rotational symmetries that are related to the number of patches as one might naively expect.

6 Summary

Within this thesis we have investigated a model of patchy particles focusing on two different topics. First, we examined the question whether decagonal and octagonal quasicrystals can be formed using the patchy particle model and secondly, we examined the growth of dodecagonal quasicrystals with patchy particles and compared it to the results for isotropic particles. The simulations concerning isotropic particles were done by M. Martinsons.

We have reproduced the dodecagonal quasicrystal which consists of particles exhibiting five patches at a rather wide patch width. This is quite astonishing, as the symmetry of the particle does not match the symmetry of the quasicrystal. In contrast to these observations we find two metastable quasicrystals, i.e. a decagonal and an octagonal quasicrystal for particles that do exhibit the according symmetry, i.e. particles with ten and eight patches. In both cases the quasicrystal is metastable for narrow patch widths. Note that the decagonal quasicrystal is only metastable when we support the short length scale of the quasicrystal whereas the octagonal quasicrystal only is metastable when we support the long length scale.

Concerning the growth of dodecagonal quasicrystals with isotropic and patchy particles we find that both systems form almost perfect quasicrystals. However, regarding patchy particles we observe regions of phononic or phasonic displacements that are connected to dislocations in some cases.

7 Outlook

So far we use the model of patchy particles to investigate the formation of different structures and the growth of quasicrystals. Now, we want to give a first impression of using patchy particles to study gels. In order to tackle this topic with our simulations, we use our sedimentation algorithm to grow a network-like structure. Then, we fix the lower- and uppermost particles and employ Brownian dynamics on the particles. Again, we use periodic boundaries in x- and open boundaries in y-direction. We use particles exhibiting five patches (see eq. 3.4) and apply the same potential parameters as previously, i.e. $r_0 = 1$ and $\sigma_{pw} = 0.49$.

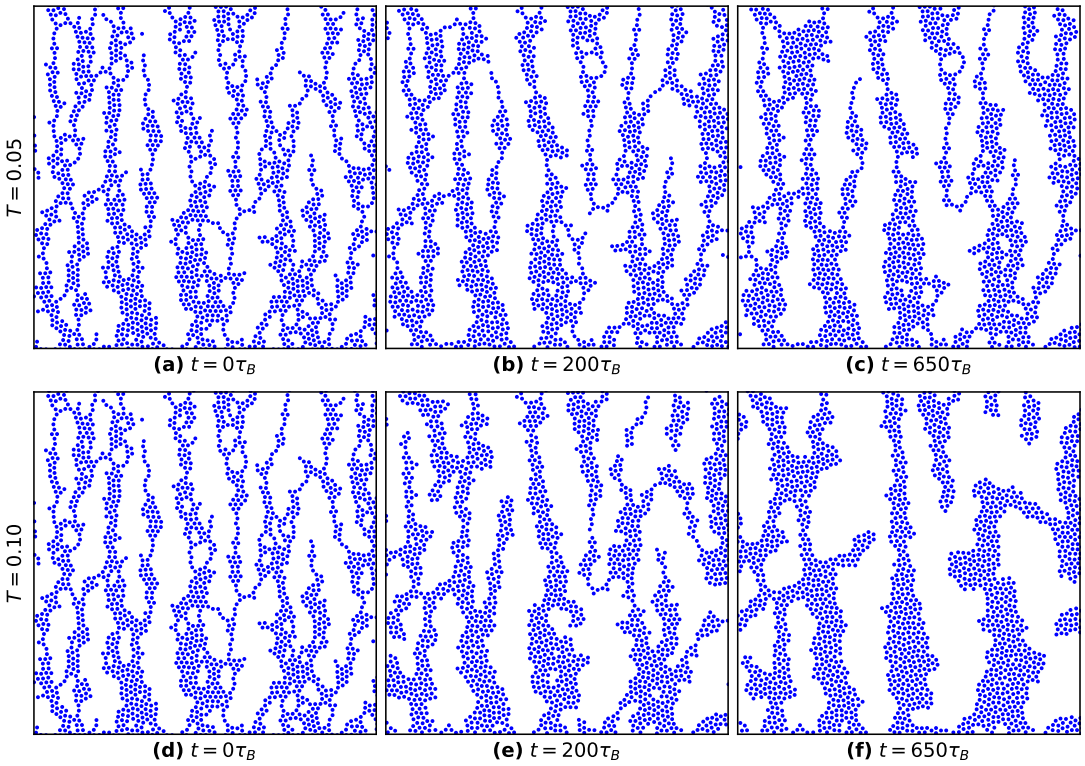

Figure 7.1: Time evolution of gel-like systems at temperature $T = 0.05$ **(a-c)** and at temperature $T = 0.1$ **(d-f)**.

Figure 7.1 indicates the time evolution of such structures at temperatures of $T = 0.05$ and $T = 0.1$. In both cases we observe that thin strands, i.e.

strands consisting of one-particle thick chains, merge with other strands. With increasing temperature this clustering of particles occurs faster. At temperature $T = 0.1$ and $t = 650\tau_B$ there are no thin strands left, furthermore, all small holes have vanished. At $T = 0.05$ this process is slower such that one can still observe several small holes and thin branches at $t = 650\tau_B$. Especially thin branches that are free on one side, i.e. the top sway. In future works, it may be interesting to do further simulations and analyse the behaviour of these structures in order to study the ageing of gels and the coarsening of foams with patchy particles.

Bibliography

[1] Nobel prize in chemistry 2011 (D. Shechtman). `https://www.nobelprize.org/prizes/chemistry/2011/press-release/`. Accessed: 9/28/2018.

[2] John Bamberg, Grant Cairns, and Devin Kilminster. The crystallographic restriction, permutations, and goldbach's conjecture. *The American mathematical monthly*, 110(3):202–209, 2003.

[3] Esther Belin and Didier Mayou. Electronic properties of quasicrystals. *Physica Scripta*, 1993(T49A):356, 1993.

[4] Emanuela Bianchi, Ronald Blaak, and Christos N Likos. Patchy colloids: state of the art and perspectives. *Physical Chemistry Chemical Physics*, 13(14):6397–6410, 2011.

[5] J Cai, JP Townsend, TC Dodson, PA Heiney, and AM Sweeney. Eye patches: Protein assembly of index-gradient squid lenses. *Science*, 357(6351):564–569, 2017.

[6] Julie A Champion, Yogesh K Katare, and Samir Mitragotri. Particle shape: a new design parameter for micro-and nanoscale drug delivery carriers. *Journal of Controlled Release*, 121(1-2):3–9, 2007.

[7] Thuy T Chastek, Steven D Hudson, and Vincent A Hackley. Preparation and characterization of patchy particles. *Langmuir*, 24(24):13897–13903, 2008.

[8] Qian Chen, Sung Chul Bae, and Steve Granick. Directed self-assembly of a colloidal kagome lattice. *Nature*, 469(7330):381, 2011.

[9] Ch Dilger, R Mikulla, J Roth, and H-R Trebin. Simulation of shear stress in icosahedral quasicrystals. *Philosophical Magazine A*, 75(2):425–441, 1997.

[10] Günther Doppelbauer, Emanuela Bianchi, and Gerhard Kahl. Self-assembly scenarios of patchy colloidal particles in two dimensions. *Journal of Physics: Condensed Matter*, 22(10):104105, 2010.

[11] Tomonari Dotera. Quasicrystals in soft matter. *Israel Journal of Chemistry*, 51(11-12):1197–1205, 2011.

[12] K Edagawa. Dislocations in quasicrystals. *Materials Science and Engineering: A*, 309:528–538, 2001.

[13] Michael Engel. *Dynamics and defects of complex crystals and quasicrystals: perspectives from simple model systems*. PhD thesis, University of Stuttgart, 2008.

[14] Michael Engel and Hans-Rainer Trebin. Self-assembly of monatomic complex crystals and quasicrystals with a double-well interaction potential. *Physical review letters*, 98(22):225505, 2007.

[15] Michael Engel, Masahiro Umezaki, Hans-Rainer Trebin, and Takashi Odagaki. Dynamics of particle flips in two-dimensional quasicrystals. *Physical Review B*, 82(13):134206, 2010.

[16] Sharon C Glotzer and Michael J Solomon. Anisotropy of building blocks and their assembly into complex structures. *Nature materials*, 6(8):557, 2007.

[17] Reinhard Hentschke. *Statistische Mechanik: Eine Einführung für Physiker, Chemiker und Materialwissenschaftler*. John Wiley & Sons, 2012.

[18] J Hielscher, M Martinsons, M Schmiedeberg, and SC Kapfer. Detection of phonon and phason modes in intrinsic colloidal quasicrystals by reconstructing their structure in hyperspace. *Journal of Physics: Condensed Matter*, 29(9):094002, 2017.

[19] Liron Korkidi, Kobi Barkan, and Ron Lifshitz. Analysis of dislocations in quasicrystals composed of self-assembled nanoparticles. In *Aperiodic Crystals*, pages 117–124. Springer, 2013.

[20] Marián Krajčí and J Hafner. Structure, stability, and electronic properties of the i-alpdmn quasicrystalline surface. *Physical Review B*, 71(5):054202, 2005.

[21] Robert Langer and David A Tirrell. Designing materials for biology and medicine. *Nature*, 428(6982):487, 2004.

[22] CM Liddell, CJ Summers, and AM Gokhale. Stereological estimation of the morphology distribution of zns clusters for photonic crystal applications. *Materials characterization*, 50(1):69–79, 2003.

[23] Weining Man, Mischa Megens, Paul J Steinhardt, and Paul M Chaikin. Experimental measurement of the photonic properties of icosahedral quasicrystals. *Nature*, 436(7053):993, 2005.

[24] M Martinsons and M Schmiedeberg. Growth of two-dimensional decagonal colloidal quasicrystals. *Journal of Physics: Condensed Matter*, 30(25):255403, 2018.

[25] Nicholas Metropolis, Arianna W Rosenbluth, Marshall N Rosenbluth, Augusta H Teller, and Edward Teller. Equation of state calculations by fast computing machines. *The journal of chemical physics*, 21(6):1087–1092, 1953.

[26] Nicholas Metropolis and Stanislaw Ulam. The monte carlo method. *Journal of the American statistical association*, 44(247):335–341, 1949.

[27] Ralf Mikulla, J Stadler, F Krul, H-R Trebin, and P Gumbsch. Crack propagation in quasicrystals. *Physical review letters*, 81(15):3163, 1998.

[28] Keisuke Nagao, Tomoaki Inuzuka, Kazue Nishimoto, and Keiichi Edagawa. Experimental observation of quasicrystal growth. *Physical review letters*, 115(7):075501, 2015.

[29] Kostya S Novoselov, Andre K Geim, Sergei V Morozov, DA Jiang, Y_ Zhang, Sergey V Dubonos, Irina V Grigorieva, and Alexandr A Firsov. Electric field effect in atomically thin carbon films. *Science*, 306(5696):666–669, 2004.

[30] Mark Oxborrow and Christopher L Henley. Random square-triangle tilings: A model for twelvefold-symmetric quasicrystals. *Physical Review B*, 48(10):6966, 1993.

[31] Francis Perrin. Mouvement brownien d'un ellipsoide-i. dispersion diélectrique pour des molécules ellipsoidales. *Journal de Physique et le Radium*, 5(10):497–511, 1934.

[32] Francis Perrin. Mouvement brownien d'un ellipsoide (ii). rotation libre et dépolarisation des fluorescences. translation et diffusion de molécules ellipsoidales. *Journal de Physique et le Radium*, 7(1):1–11, 1936.

[33] Carolyn L Phillips, Eric Jankowski, Bhaskar Jyoti Krishnatreya, Kazem V Edmond, Stefano Sacanna, David G Grier, David J Pine, and Sharon C Glotzer. Digital colloids: reconfigurable clusters as high information density elements. *Soft Matter*, 10(38):7468–7479, 2014.

[34] Carolyn L Phillips, Eric Jankowski, Michelle Marval, and Sharon C Glotzer. Self-assembled clusters of spheres related to spherical codes. *Physical Review E*, 86(4):041124, 2012.

[35] Aleks Reinhardt, Flavio Romano, and Jonathan PK Doye. Computing phase diagrams for a quasicrystal-forming patchy-particle system. *Physical review letters*, 110(25):255503, 2013.

[36] Aleks Reinhardt, John S Schreck, Flavio Romano, and Jonathan PK Doye. Self-assembly of two-dimensional binary quasicrystals: A possible route to a dna quasicrystal. *Journal of Physics: Condensed Matter*, 29(1):014006, 2016.

[37] Matthias Sandbrink. *Tailored Colloidal Quasicrystals*. PhD thesis, HHU Düsseldorf, 2015.

[38] Matthias Sandbrink and Michael Schmiedeberg. Course of dislocation lines in templated three-dimensional colloidal quasicrystals. *Physical Review B*, 90(6):064108, 2014.

[39] Michael Schmiedeberg. *Colloidal particles on quasicrystalline substrates*. PhD thesis, TU Berlin, 2008.

[40] D. Shechtman, I. Blech, D. Gratias, and J. W. Cahn. Metallic phase with long-range orientational order and no translational symmetry. *Phys. Rev. Lett.*, 53:1951–1953, Nov 1984.

[41] Joshua ES Socolar, TC Lubensky, and Paul J Steinhardt. Phonons, phasons, and dislocations in quasicrystals. *Physical Review B*, 34(5):3345, 1986.

[42] Walter Steurer. Why are quasicrystals quasiperiodic? *Chemical Society Reviews*, 41(20):6719–6729, 2012.

[43] Lei Tian, Xue Li, Dewei Wan, Zafar Ali, and Qiuyu Zhang. Large-scale fabrication of polymer ellipsoids with controllable patches via the viscosity-induced deformation of spherical particles. *Polymer Chemistry*, 8(25):3774–3777, 2017.

[44] Elisabeth Tondl, Malcolm Ramsay, Peter Harrowell, and Asaph Widmer-Cooper. Defect-mediated relaxation in the random tiling phase of a binary mixture: Birth, death and mobility of an atomic zipper. *The Journal of chemical physics*, 140(10):104503, 2014.

[45] Marjolein N van der Linden, Jonathan PK Doye, and Ard A Louis. Formation of dodecagonal quasicrystals in two-dimensional systems of patchy particles. *The Journal of chemical physics*, 136(5):054904, 2012.

[46] Z Valy Vardeny, Ajay Nahata, and Amit Agrawal. Optics of photonic quasicrystals. *Nature photonics*, 7(3):177, 2013.

[47] Stephen Whitelam. Minimal positive design for self-assembly of the archimedean tilings. *Physical review letters*, 117(22):228003, 2016.

[48] TA Witten Jr and Leonard M Sander. Diffusion-limited aggregation, a kinetic critical phenomenon. *Physical review letters*, 47(19):1400, 1981.

[49] Allison M Yake, Charles E Snyder, and Darrell Velegol. Site-specific functionalization on individual colloids: Size control, stability, and multilayers. *Langmuir*, 23(17):9069–9075, 2007.

[50] Y-P Zhao, D-X Ye, Pei-I Wang, G-C Wang, and T-M Lu. Fabrication of si nanocolumns and si square spirals on self-assembled monolayer colloid substrates. *International Journal of Nanoscience*, 1(01):87–97, 2002.

Self-citation

Sections 5.2 and 5.3 are taken from our paper

Growth of two-dimensional dodecagonal colloidal quasicrystals: Particles with isotropic pair interaction with two length scales vs. patchy colloids with preferred binding angles by Anja Gemeinhardt, Miriam Martinsons, and Michael Schmiedberg in the version that was submitted to *Eur. Phys. J. E* on 9/18/2018.
All simulations regarding isotropic particles were done by M. Martinsons, all simulations regarding patchy particles were done by A. Gemeinhardt.

Acknowledgements

Foremost I would like to thank my supervisor Prof. Dr. Michael Schmiedeberg for his continuous support and guidance. Besides my supervisor, I would also like to thank Miriam Martinsons for all the discussions and motivation throughout the year. Furthermore, I thank all the other members of the chair for the friendly and fun atmosphere.
Last but not least, I also thank my family and my friends for all their support during my studies.

Statutory declaration

I hereby confirm that I have written the accompanying thesis by myself, without contributions from any sources other than those cited in the text. This thesis was not submitted to any other authority to achieve an academic grading and was not published elsewhere.

Erlangen, 10/5/2018
place, date

A. Gemeinhardt